

**STUDIES ON THE GROWTH, STRUCTURAL AND  
ELECTRICAL PROPERTIES OF SILICON-BASED  
HETEROSTRUCTURE NANOWIRES**

**QIAN GUANGHAN**

**FACULTY OF SCIENCE  
UNIVERSITY OF MALAYA  
KUALA LUMPUR  
2015**

**STUDIES ON THE GROWTH, STRUCTURAL AND  
ELECTRICAL PROPERTIES OF SILICON-BASED  
HETEROSTRUCTURE NANOWIRES**

**QIAN GUANGHAN**

**DISSERTATION SUBMITTED IN FULFILMENT  
OF THE REQUIREMENTS  
FOR THE DEGREE OF MASTER SCIENCE**

**FACULTY OF SCIENCE  
UNIVERSITY OF MALAYA  
KUALA LUMPUR  
2015**

# UNIVERSITI MALAYA

## ORIGINAL LITERARY WORK DECLARATION

Name of Candidate: **QIAN GUANGHAN**  
I/C/Passport No: **G42001151**  
Registration/Matric No.: **SGG130002**  
Name of Degree: **MASTER OF TECHNOLOGY (MATERIALS SCIENCE)**

Title of Project Paper/Research Report/Dissertation/Thesis ("this Work"):

**"STUDIES ON THE GROWTH, STRUCTURAL AND ELECTRICAL PROPERTIES OF SILICON-BASED HETEROSTRUCTURE NANOWIRES"**

Field of Study: **NANOTECHNOLOGY AND NANOMATERIALS**

I do solemnly and sincerely declare that:

- (1) I am the sole author/writer of this Work,
- (2) This Work is original,
- (3) Any use of any work in which copyright exists was done by way of fair dealing and for permitted purposes and any excerpt or extract from, or reference to or reproduction of any copyright work has been disclosed expressly and sufficiently and the title of the Work and its authorship have been acknowledged in this Work,
- (4) I do not have any actual knowledge nor do I ought reasonably to know that the making of this work constitutes an infringement of any copyright work,
- (5) I hereby assign all and every rights in the copyright to this Work to the University of Malaya ("UM"), who henceforth shall be owner of the copyright in this Work and that any reproduction or use in any form or by any means whatsoever is prohibited without the written consent of UM having been first had and obtained,
- (6) I am fully aware that if in the course of making this Work I have infringed any copyright whether intentionally or otherwise, I may be subject to legal action or any other action as may be determined by UM.

(Candidate Signature)

Date:

Subscribed and solemnly declared before,

Witness's Signature

Date:

Name:

Designation:

## ABSTRACT

This work reports the investigation of Ni catalyzed Si-based nanowires grown by hot-wire chemical vapor deposition at different filament temperatures on crystal Si (c-Si) and glass substrates. These nanowires include NiSi, NiSi/Si core-shell and NiSi/SiC core-shell nanowires that grown by varying the filament temperature,  $T_f$ . The NiSi nanowires were grown at lowest  $T_f$  of 1150°C. At  $T_f$  of 1450°C, the nanowires were structured by crystalline Si and amorphous Si which Si attributed to the core and shell of the nanowires, respectively. The nanowires exhibited NiSi/SiC heterostructure core-shell nanowires with increase in  $T_f$  to 1850°C. The morphological properties of these nanowires were strongly dependent on the substrate and filament temperature. The nanowires grown on c-Si substrate showed a better alignment and a higher density as compared to the nanowires grown on glass substrate. The effect of hydrogen heat transfer by the filament temperature demonstrated a phase change from NiSi to Ni<sub>2</sub>Si with increase in filament temperature. The increasing of filament temperature enhances gas phase reactions thus generates more SiC clusters which consequently formed the SiC shell. These NiSi/SiC core-shell nanowires were structured by single crystalline NiSi and amorphous SiC respectively. The roles of the filament temperature on the growth and constituted phase change of the nanowires are discussed in detail. Last but not least, the core-shell nanowires exhibited a significant hetero-junction electrical characteristic which could be a great potential application in nano-diode devices.

**Keywords:** Heterostructure, core-shell nanowires, HWCVD, SiC, NiSi

## **ABSTRAK**

Ni-bermangkin Si berasaskan heterostruktur nanowayar ditumbuh di atas kristal Si substrat oleh wayar panas wap kimia pemendapan (HWCVD) telah dikaji. Ini termasuk heterostruktur nanowayar NiSi, amorfus/kristal Si nanowayar teras-tempurung dan NiSi/SiC nanowayar teras-tempurung yang berkembang dengan mengubah suhu filamen,  $T_f$ . Pada  $T_f$  1450°C, heterostruktur nanowayar terbentuk oleh kristal dan amorfus Si yang berpunca daripada teras dan tempurung nanowayar masing-masing. Morfologi nanowayar menunjukkan perubahan ketara dengan peningkatan suhu filamen. Selain itu, pemindahan haba hidrogen oleh suhu filamen menunjukkan perubahan fasa dari NiSi kepada Ni<sub>2</sub>Si dengan peningkatan suhu filamen. Peningkatan suhu filamen juga meningkatkan tindak balas fasa gas yang menjana lebih banyak kelompok SiC dan seterusnya membentuk NiSi/SiC nanowayar teras-tempurung pada 1850°C. Peranan suhu filamen pada pertumbuhan dan perubahan fasa nanowayar turut dibincangkan. Ciri-ciri elektrik yang terdapat pada nanowayar turut dipersembahkan.

**Kata Kunci:** Heterostruktur nanowayar, Wayar panas wap kimia pemendapan (HWCVD), pertumbuhan Nanowayar.

## **ACKNOWLEDGEMENT**

I would like to express my sincere gratitude and thanks to my supervisor, Dr. Goh Boon Tong for guiding and advising me throughout this work. Profuse thanks to him for being patient and understanding. Without his criticism, comments, timely aid and intervention this study may not have materialized.

Also, I would like to thank all the members of Low Dimensional Materials Research Centre, Department of Physics in University of Malaya members for guiding me, giving suggestions, ideas, and support. Among them includes Nur Fatin Farhanah binti Nazaruddin, Najwa binti Hamzan and Farah Nadiah binti Nordin. The experiences with them have been wonderful, interesting and rewarding.

This work was supported by the University of Malaya Research Grant (UMRG) of RG259-13AFR and the University of Malaya Postgraduate Research Fund (PPP) of PO032-2014A.

## TABLE OF CONTENTS

	<i>Page</i>
<i>Abstract</i>	iii
<i>Acknowledgement</i>	v
<i>Table of Contents</i>	vi
<i>List of Figures</i>	viii
<i>List of Tables</i>	xii
<i>List of Symbols and Abbreviations</i>	xiii
 <b>Chapter 1</b>	
<b>INTRODUCTION</b>	
1.1 Background	1
1.2 Problem statement	6
1.3 Motivation of this work	7
1.4 Objectives	7
1.5 Thesis overview	8
 <b>Chapter 2</b>	
<b>LITERATURE REVIEW</b>	
2.1 Nanomaterials and nanotechnology	9
2.2 One-dimensional NiSi and SiC nanowire	10
2.3 Nanowire diode	19
2.3 Hot-wire chemical vapor deposition (HWCVD)	19
2.4 Nanowire grow mechanism	24
 <b>Chapter 3</b>	
<b>METHODOLOGY</b>	
3.1 Introduction	31
3.2 Hot-wire chemical vapour deposition	31
3.2.1 Vacuum chamber	33
3.2.2 Plasma generator	33
3.2.3 Hot-wire supply	34
3.2.4 Vacuum system	35
3.2.5 Gas supply	36
3.2.6 Heating supply	37

3.3	Experiment method	38
	3.3.1 Substrate cleaning	38
	3.3.2 Pre-heating of filament	39
	3.3.3 Ni evaporation	40
	3.3.4 Deposition	41
3.4	Characterization techniques	43
	3.4.1 Scanning electron microscope (SEM)	43
	3.4.2 Energy dispersive X-ray (EDX)	43
	3.4.3 Transmission electron microscope (TEM)	44
	3.4.4 X-ray diffraction (XRD)	46
	3.4.5 Raman spectroscopy	47
	3.4.5 I-V measurement	48
<b>Chapter 4</b>	<b>RESULTS AND DISCUSSIONS</b>	
4.1	Effects of filament temperature on substrate surface temperature	50
4.2	Surface morphologies of nanowires	51
4.3	Cross-sectional view study	56
4.4	Microstructure study	59
4.5	Compositions studies of a single nanowire by EDS elemental mappings	62
4.6	Phases and orientation studies	63
4.7	Structural properties study	67
4.8	Optical properties study by photoluminescence emission spectra	69
4.9	Electrical properties study	71
<b>Chapter 5</b>	<b>CONCLUSIONS</b>	
5.1	Conclusions	75
	<b>REFERENCES</b>	77



## LIST OF FIGURES

		<i>Page</i>
Figure 1.1	Different structure of one-dimension nanowires.	3
Figure 2.1	(a)~(b) SEM and (c)~(d) TEM image of NiSi Nanowire growth by MIG.	12
Figure 2.2	Raman spectrum of the NiSi nanowires.	13
Figure 2.3	Typical SEM images of SiC nanowires.	15
Figure 2.4	(a)~(b) Typical TEM images of a single SiC nanowire. (c)~(d) corresponding SAED pattern and HRTEM image of the SiC nanowire.	16
Figure 2.5	(a) A typical EDS spectrum of SiC nanowires. The inset is an enlarged spectrum. (b)~(c) The element maps of Si and C of a single nanowire.	16
Figure 2.6	XRD pattern of SiC nanowires.	17
Figure 2.7	Raman spectrum of the SiC nanowires	18
Figure 2.8	SiH <sub>4</sub> deposit process of hot-wire chemical vapour deposition.	22
Figure 2.9	(a) Mode fraction and (b) infrared absorption intensities of C <sub>2</sub> H <sub>2</sub> and CH <sub>4</sub> as a function of filament temperature.	24
Figure 2.10	(a) Periodic table with potential catalyst metals classified according to their phase diagram. (b) Minimum temperature of certain metals required for vapor-liquid-solid (VLS) growth of Si nanowires.	26
Figure 2.11	Schematic illustration for the growth of nanowires with on the VLS mechanism.	28
Figure 2.12	Schematic diagram and SEM image of MIG nanowire growth. (a) Groove and agglomeration of Ni layer by	30

heating, (b) Clustering during Si supply, (c) Formation of nanofibers, and (d) Growth of nanowires.

Figure 3.1	Flow chart of this work.	31
Figure 3.2	(a) Schematic diagram of the HWCVD reaction chamber. (b) Real picture of the HWCVD vacuum system.	32
Figure 3.3	Photograph of RF generator used.	34
Figure 3.4	Photograph of a process for (a) plasma treatment and (b) hot-wire decomposition of silane processes.	35
Figure 3.5	Photograph of the gas line.	37
Figure 3.6	Real pictures of (a) temperature controller and voltage regulator panels, (b) heater rod and (c) thermocouple.	38
Figure 3.7	(a) Photograph of tungsten filament. (b) photograph of setup of filament for nickel evaporation and deposition processes. Filament is placed in a filament electrode.	40
Figure 3.8	(a) Schematic diagram of Ni evaporation process. (b) Photograph of the Ni coated on glass substrates.	41
Figure 3.9	(a) Plasma treatment process to form Ni nano-island (b) Decomposition of gas precursors ( $\text{SiH}_4$ , $\text{CH}_4$ , $\text{H}_2$ ) during deposition process.	42
Figure 3.10	Hitachi SU 8000 SEM picture and schematic diagram of SEM	43
Figure 3.11	Schematic diagram of EDX basic principle. (a) generation of characteristic X-ray in sodium (Na) atom model. (b) X-ray schematic diagram.	44
Figure 3.12	JEOL JEM-2100F TEM picture and schematic diagram of TEM.	45
Figure 3.13	Schematic diagram of XRD.	47

Figure 3.14	InVia Raman microscope picture and representation of Raman scattering from particles.	48
Figure 3.15	KEITHLEY Model 236 source measure unit and electrode pins picture.	49
Figure 3.16	A schematic diagram of the fabricated Si-based nanowires heterojunction structure and the electrodes configuration.	49
Figure 4.1	Variations of substrate temperature, and substrate surface on Si and glass substrates with filament temperature.	51
Figure 4.2	FESEM images of the Si-based nanowires synthesis by HWCVD on silicon at different filament temperatures (a) 1150°C, (b) 1450°C, (c) 1650°C, (d) 1750°C, (e) 1850°C, (f) 1950°C. Insets show the high magnification image of the nanowires. (Insets bar is 500 nm).	54
Figure 4.3	FESEM images of the nanowires synthesis by HWCVD on glass at different filament temperatures. (a) 1150°C, (b) 1450°C, (c) 1650°C, (d) 1750°C, (e) 1850°C, (f) 1950°C. Insets show the high magnification image of the nanowires. (Insets bar is 500 nm).	55
Figure 4.4	Variations of nanowire diameter with filament temperature on silicon and glass substrate.	56
Figure 4.5	Cross-sectional view of FESEM images of the nanowires prepared by HWCVD at filament temperature of 1850°C. (a) secondary electron (b) backscattered electron signals (c) backscattered electron signal collected by a photo-diode backscattered electron (PDBSE) detector that attached to the SEM. Insets figures present high magnification of the FESEM images.	58
Figure 4.6	(a) TEM morphology of the NiSi/Si core-shell NWs prepared at filament temperature of 1650°C. (b) and (d) HRTEM image of the NWs enlarged from the frame in. (c) show TEM image of the side wall structures of the NWs.	61

Figure 4.7	(a) TEM morphology of the NiSi/SiC core-shell NWs prepared at filament temperature 1850°C. (b) and (d) HRTEM image of the NWs enlarged from the frame in (a) show a insert particle inside the NW.	62
Figure 4.8	(a) Brigh-field TEM image of a single nanowire, (b) ~ (e) EDS element maps of the core-shell nanowire.	63
Figure 4.9	XRD spectra of the nanowires prepared by HWCVD at different filament temperatures.	65
Figure 4.10	Weight percentage of phases presented in the samples prepared by HWCVD at different filament temperatures.	67
Figure 4.11	Raman scattering spectra of the nanowires prepared by HWCVD at different filament temperatures. (a), (c) and (e) is filament temperature 1150 ~ 1950°C on silicon substrates. (b), (d) and (f) is filament temperature 1150 ~ 1950°C on glass substrates.	69
Figure 4.12	Photoluminescence (PL) spectra for the nanowires on silicon substrate at different filament temperatures.	71
Figure 4.13	I–V curves of the samples prepared by HWCVD at different filament temperatures. Inset of the figure presents the logarithmic current against voltage ( $\ln I$ –V) plot of the NiSi/Si and NiSi/SiC core-shell nanowires prepared at filament temperatures of 1450 and 1850°C	72
Figure 4.14	Generic diode mode with parasitic series resistance and parallel conductances.	72

## LIST OF TABLES

		<i>Page</i>
Table 1	Nanowire fabrication types and conditions	27
Table 2	Deposite parameters in this work.	42
Table 3	Experimental values of the parameters obtained from I–V fittings.	74

## LIST OF SYMBOLS AND ABBREVIATIONS

C	Carbon
Ni	Nickel
Si	Silicon
O <sub>2</sub>	Oxygen
H <sub>2</sub>	Hydrogen
SiC	Silicon carbide
SiH <sub>4</sub>	Silane
CH <sub>4</sub>	Methane
NH <sub>4</sub> OH	Ammonia
HCl	Hydrochloric acid
H <sub>2</sub> O <sub>2</sub>	Hydrogen peroxide
c-Si	Crystal silicon
DI	Deionized
sccm	Standard cubic centimeters per minute
CVD	Chemical vapor deposition
HWCVD	Hot-wire chemical vapor deposition
FESEM	Field emission scanning electron microscope
EDX	Energy dispersive X-ray
HRTEM	High resolution transmission electron microscope
STEM	Scanning transmission electron microscopy
XRD	X-ray diffraction
PL	Photoluminescence
PDBSE	Photo-diode backscattered electron
HAADF	High angle annular dark field
VLS	Vapor-liquid-solid
MIG	Metal induced growth

MDG	Metal diffusion growth
$T_s$	Surface temperatures for c-Si substrate
$T_g$	Surface temperatures for glass substrate
$T_b$	Temperature on the bottom surface of the substrates
$T_f$	Filament temperature
I-V	Current-voltage

## CHAPTER 1

### INTRODUCTION

#### 1.1 Background

Semiconductor nanowires have been extensively studied due to their potential applications in a wide range of applications (Bae et al., 2010; Rurali, 2010; L. Yu et al., 2009). The hybrid heterostructures such as core-shell nanowires are expected to improve the properties of the nanowires such in the case of applications for high-temperature sensing (Bi et al., 2013), high-performance FET (field effect transistors) (Xiang et al., 2006) and enhanced hydrogen generation photocatalytic (Hao, Wang, Tong, Jin, & Guo, 2012).

Design and synthesis of multi-dimensional materials to achieve certain desirable properties is more complex. These materials are diverse structures that consisted of metals, semiconductors, carbon, which generally are axially connected to a heterojunction by two different nanomaterials. One-dimension heterostructure materials with unique properties and its functionality can be obtained for wide range of applications in various new fields.

For example, semiconductor-semiconductor p-n junction is formed to produce a rectified current logic gates (Huang, Duan, Cui, & Lieber, 2002), nano photodetector (Hayden, Agarwal, & Lieber, 2006) and multifunction light emitting diode (McAlpine, Ahmad, Wang, & Heath, 2007). Metal-semiconductor-metal heterojunction nanowires with superior optical and conductivity properties potentially can be used in biosensors (Penn, He, & Natan, 2003), gene transfer (Salem, Searson, & Leong, 2003) and



separation (K. B. Lee, Park, & Mirkin, 2004). It has been reported that metal-metal heterojunction with different fragments have different functions and features. The device prepared in this heterojunction has disadvantages in electrical properties. However, highly mismatched with no dislocation lines can formed in one-dimensional heterostructure materials. Matthews and Blakeslee et al. recently described the formation of a two-dimensional heterostructure is not critical thickness for dislocation (Matthews & Blakeslee, 1974). The model predicted that over the critical radius, nano heterojunction with instability showed a larger grain. Materials have lattice mismatch, hardly form a perfect heterojunction without dislocation. Thus, maximum advantage of the nanowire heterostructure is the size below the critical radius, inappropriate dislocation does not exist. It is possible to obtain novel, versatile and high-performance electronic devices.

Depending on the composition, the nano-heterojunction materials can be divided into follows: (1) Semiconductor-Semiconductor; (2) semiconductor-metal; (3) metal-metal; (4) carbon-carbon; (5) carbon-metal; (6) carbon-semiconductor heterojunction, wherein the “carbon” may be carbon nanotubes, amorphous carbon or diamond. According to different classification of the connections, it include a segment-type, a core-shell, cross-type, branch heterojunction type and brushes as shown in Fig. 1.1 (Mieszawska, Jalilian, Sumanasekera, & Zamborini, 2007). These heterojunctions play an important role in their properties. There are some synthesis methods of the material, for example, template synthesis structure and core-shell heterostructure. This thesis focuses the core-shell heterostructure materials.

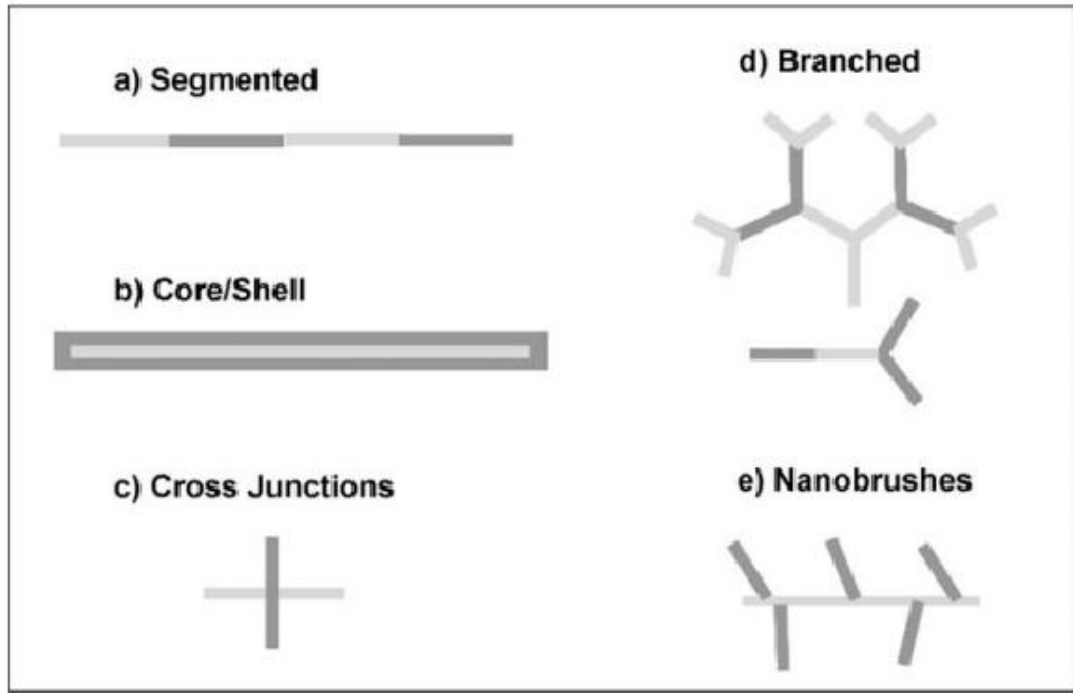


**Fig. 1.1** Different structure of one dimension nanowires (Mieszawska et al., 2007).

Recently, silicon carbide (SiC) has gained extensive interests in coating and micro-electromechanical systems (MEMS) (Mehregany, Zorman, Roy, Fleischman, & Rajan, 2000; Sarro, 2000). SiC is generally used in high-power applications, harsh environment such as wider high temperature and radiation condition. SiC has been greatly employed in mechanical toughness and high fracture strength, because of the high Si-C bond are capable of imparting high Young's modulus (X. Li & Bhushan, 1999). Moreover, SiC is a chemically inert material to most corrosive and aggressive chemical substance, and biocompatible material (Casady & Johnson, 1996; Willander, Friesel, Wahab, & Straumal, 2006; Yakimova et al., 2007). The existence of more than 100 types of poly silicon carbide in the cubic phase SiC (3C-SiC), they can be deposited on Si. so it has drawn particular attention in researchs (Marshall, 1974). SiC nanostructures are known with their excellent properties such as high thermal

conductivity, high mechanical properties, good thermal shock resistance, low thermal expansion coefficient, as well as its chemical stability and electron affinity, allowing them working in harsh environments (J. Fan, Wu, & Chu, 2006; Wong, Sheehan, & Lieber, 1997). By incorporated highly metallic properties of single crystalline NiSi into the NiSi/SiC core-shell nanowires, that expected to enhance the electrical and optical properties of this heterostructure material in various applications. The NiSi core electrode could use as 1D electrodes for enhancing the efficiency of electron transfer between current collector supports and individual electrode materials and ion transport to the electrode (C. J. Kim et al., 2007; Yue Wu, Xiang, Yang, Lu, & Lieber, 2004). Moreover, this metallic/semiconductor heterostructures probably could enhance the carry mobilities which would significantly improve the performance of existing nanowires-based devices (Lauhon, Gudiksen, Wang, & Lieber, 2002).

Recently, extensive works have been carried up to investigate the properties of Si-based heterostructures. they using various deposition techniques include chemical vapor deposition (CVD), hot-wire chemical vapor deposition (HWCVD), lithography and laser ablation (Bandaru & Pichanusakorn, 2010; H. J. Fan, Werner, & Zacharias, 2006; Rao, Deepak, Gundiah, & Govindaraj, 2003; Suzuki, Araki, Tosa, & Noda, 2007). In this work, the Si-based heterostructure nanowires have been grown by HWCVD at different filament temperatures. HWCVD is a preferable technique for the fabrication of Si-based nanowires with lower cost production and large-area deposition. Moreover, HWCVD also capable in generating high density of grow precursors ( $\text{SiH}_3$  and  $\text{CH}_3$ ) by using high temperature tungsten filament as a catalyst. In the HWCVD, the filament temperature is playing an important role in controlling the decomposition of the source

gas and the gas phase reactions during the deposition. Decomposition of the SiH<sub>4</sub> and CH<sub>4</sub> are at different filament temperatures, in terms of SiH<sub>4</sub> it starts to decompose at 1027°C and the decomposition rate increases dramatically when the temperature is above 1427°C (Tange, Inoue, Tonokura, & Koshi, 2001). While, the moderate decomposition of CH<sub>4</sub> happens at 1750°C and above (Komura et al., 2007; Tabata & Komura, 2007). The grow mechanism of NiSi/SiC core-shell nanowire involve process of SiH<sub>4</sub> and CH<sub>4</sub> decompose, gas phase reactions and the surface reactions, all above processes lead to the growth of nanowires. The quality of sample is highly influenced by the gas phase (SiH<sub>4</sub>, CH<sub>4</sub>, H<sub>2</sub> molecules and radicals) reactions. The filament temperature plays an important role in controlling the gas phase reactions (Tange et al., 2001). In SiH<sub>4</sub>/CH<sub>4</sub>/H<sub>2</sub> system, the decomposition of SiH<sub>4</sub> and the desorption of Si and H radicals form the HW surface at a threshold T<sub>f</sub> of 1450°C. That generally agreed upon by several reported studies (Doyle, Robertson, Lin, He, & Gallagher, 1988; Matsumura, 1986). In that temperature the Si and H radicals desorbed rapidly in large quantities. When the surface of filament is heated to more than 1750°C, the precursors (CH<sub>4</sub>, SiH<sub>4</sub> and H<sub>2</sub>) molecules decomposed onto the surface of hot filament. CH<sub>4</sub> decompose to CH<sub>3</sub> molecules takes place mainly through gas phase reaction:  $\text{CH}_4 + \text{H} \rightarrow \text{CH}_3 + \text{H}_2$  (Komura et al., 2007; Komura, Tabata, Narita, & Kondo, 2008; Tabata & Komura, 2007). These observations on the gas phase reactions involving active radicals in a HWCVD process are very useful when studying the role of filament temperature in synthesizing Si and SiC base nanowires.

The structural and electrical properties of the as-grown Si heterostructure nanowires were investigated. The physical and chemical properties of the nanowires

such as morphological, microstructure and compositions were investigated by field emission scanning electron microscopy (FESEM), high resolution transmission electron microscopy (HRTEM), X-ray diffraction (XRD) and micro-Raman scattering spectroscopy. Current-voltage (I-V) characteristics were used to analyze electrical properties of the nanowires.

## **1.2 Problem statement**

Generally, the single-phased intrinsic materials generally have low conductivity, weak mechanical stability and associated side reactions due to their unprotected surfaces, which make them unsuitable for various device applications (Fu et al., 2006; Liu, Li, Ma, & Cheng, 2010). These disadvantages has made the nanowires lack of interest in applications energy conversion and storage. Therefore, hybrid core-shell nanowires have become new approach for these applications. The incorporation of highly metallic properties of single-crystalline NiSi nanowires as core electrodes into the NiSi/SiC core-shell is expected to enhance their electrical and optical properties. The NiSi core electrodes could be used as 1D electrodes for enhancing the efficiency of electron transfer between the current collector supports and individual electrode materials as well as of ion transport to the electrode (Cohen-Karni et al., 2012; Yue Wu, Xiang, et al., 2004). Moreover, this metallic/semiconductor heterostructure could possibly enhance the carrier mobility which would significantly improve the performance of the existing nanowire-based devices.

### **1.3 Motivation of this work**

Si-based nanostructures such as nanowires, nanorods and nanotubes have attracted more and more attention due to their applications in nanoscale devices. One-dimensional materials are excellent in electrical, optical and magnetic properties. Hence, there great potential to be used in nanoelectronics, photonics, laser plasma, medical diagnostics, drug delivery and chemical sensors. SiC is a wide band gap semiconductor used for high temperature, high power applications and radiation-hard environment. By incorporated highly metallic properties of single crystalline NiSi nanowires as a core electrode into the NiSi/SiC core-shell nanowires is expected to enhance the electrical and optical properties of this heterostructures material in various applications. The NiSi core is believed to be able in boost the efficiency of electron transfer between current collector supports and individual electrode materials, as well as that of ion transport to the electrode. Moreover, this metallic/semiconductor heterostructure probably could enhance the carrier mobilities, which would significantly improve the performance of existing nanowires-based devices.

### **1.4 Objectives**

The objectives of this research are:

- 1) To investigate the role of filament temperature on the growth of Ni-catalyzed Si-based core-shell nanowires by HWCVD on c-Si and glass substrates,
- 2) To analyze the structural, optical and electrical properties of the nanowires,

## **1.5 Thesis overview**

This thesis is organized mainly into five chapters. The first chapter describes the introduction of one-dimensional core-shell nanowires included the objectives, motivation of the work and also an outline of the report. Chapter 2 presents the literature review of this work. The description of the advantages of nickel silicide, silicon carbide and heterostructure of nanowires also include in this chapter. Also discuss the importance of using HWCVD system. Chapter 3 details description on the research methodology include the experimental setup, material used and characterization techniques of this work. Chapter 4 present the results and discussion of this work. Chapter 5 is summary and conclusion of the work done in this work.

## **CHAPTER 2**

### **LITERATURE REVIEW**

#### **2.1 Nanomaterials and Nanotechnology**

When the size of particles is 0.1 micron (100 nm) or less, the unit is generally nano. The physical and chemical properties are significantly different from normal size. Nanotechnology studies the characteristics and interactions in the range of 0.1 to 100 nm. Nanotechnology research indicates that macro to micro of an object is made, a large size to a small size, and also the nano-micron level of development. Numerous studies have showed a number of specific physical, chemical and biological properties exhibited differently when the size of the material is at the nanometer level, from the material at the macroscopic state that reflect the nature of the special nature of these nanoscale that emerging into high technology industries (Kalantar-zadeh & Fry, 2007).

Due to nanoscale dimensions, nanomaterials exhibit small size effect, quantum tunneling effect, Coulomb blockade effects and surface effects due to the fluctuations between the electrons and atomic interactions of nanomaterials. Nanomaterials possess properties that many of the materials do not have especially in the physical, chemical and biological properties. Due to surface effects, as in the reduction in particle size of nano-materials, a sharp increase in specific surface area of the material, the number of atoms in the proportion of the surface of the bulk atoms is also greatly increased, while the surface energy and the surface tension increases, which causes nanomaterials change in nature. As the particle diameter becomes smaller, the specific surface area will be significantly increased, the number of surface atoms is also increasing rapidly. For



instance, a particle size of 10 nm with the specific surface area of 90 m<sup>2</sup>/g; when the particle diameter is 5 nm, the specific surface area of 180 m<sup>2</sup>/g, the number of surface atoms to account for 50 %, particle size down to 2 nm, specific surface area soared to 450 m<sup>2</sup>/g, the number of surface atoms to 80 %. The surface atomic ratio of the total number of nanomaterials atoms will increase rapidly when the size of nano-material is reduced to 10 nm or less. The surface on these atoms nanomaterials have high activity, very unstable, and very easy to combine with other atoms. The metal nanoparticles in the air easily burn the inorganic nanoparticles when it is exposed to the gas in the air in which it will absorb and react. This feature has been used to construct miniature sensors and detectors. As the size of the amount gradually reaching the nanoscale under certain critical conditions, some changes can cause to the nature. The effects when the coherence of length of nanomaterials size and light wavelength, the de Broglie wavelength or superconducting state or transmitted physical characteristics and depth dimensions comparable or smaller are that the periodic boundary conditions of the crystal material will be destroyed, the electronic transport behaviour received limitations, the electron mean free path is shortened, and the coherence of electrons localized enhancements, resulting nanomaterials there are special sound, light, electricity, magnetic, thermal, mechanical and other properties (Wan et al., 2009; Xia et al., 2003; R. Yan, Gargas, & Yang, 2009).

## **2.2 One-dimensional NiSi and SiC nanowire**

Silicide is silicon compound with a metal as electropositive component (J. Kim & Anderson, 2005). It can reduce the resistivity of local-interconnect metallization and

gate and is commonly used in silicon based microelectronics.  $\text{CoSi}_2$  and  $\text{TiSi}_2$  are some popular silicide candidates (Han, Liu, & Zhao, 2015), however there are some limitations. For example  $\text{TiSi}_2$  line width and the sheet resistance of the display depends  $\text{C}_{49}$  phase. Therefore it is difficult to transit to a low resistivity  $\text{C}_{54}$  phase.  $\text{CoSi}_2$  film consumes more Si compared  $\text{TiSi}_2$  (Colgan, Gambino, & Cunningham, 1996). Presented in nickel siliciden ( $\text{NiSi}$ ), some of the advantages of low resistivity, lower Si consumption and the formation of a relatively low temperature, and therefore it is a promising material to replace those silicide material (G. B. Kim et al., 2003).  $\text{NiSi}$  has been used as an ideal source for electrical contact materials and recently the  $\text{NiSi}$  provided the drain and gate complementary metal oxide silicon devices. In addition, they also exhibit superior performance to reduce the proportion of (Lavoie, d'Heurle, Detavernier, & Cabral, 2003).

There has been abundance reported on  $\text{NiSi}$  nanowire growths. Metal-induced growth (MIG) method is a unique nanowire growth mechanism that the  $\text{NiSi}$  nanowire follows (J. Kim & Anderson, 2005). Highly straight  $\text{NiSi}$  nanowires grown by a sputtering method at  $575^\circ\text{C}$  followed a solid-phase reaction of Ni and Si (J. Kim, 2010). Low temperature process is preferably applied as a nanowire interconnected with the structure of the manufactured nanoscale little or no damage. MIG has advantage among a growing number of epitaxial Si film, which uses solid phase crystallization and solid phase epitaxy mechanisms. The behavior of the deposited metal catalyst film which act as a seed layer, the sputtering silicon interact to form a silicide layer on top of it grown Si film. Nickel and cobalt are commonly used as metal catalyst in MIG method. Si epitaxial film growth and to exhibit the spontaneous formation of a good ohmic contact

layer, a thin film or small  $\text{CoSi}_2$  and  $\text{NiSi}_2$  lattice mismatch provides an excellent precursor layer. MIG method is rapid crystallization of silicon at low temperature and methods cultured versatile applications in Si. NiSi nanowires growth by MIG as demonstrated by scanning electron microscope (SEM) and transmission electron microscope (TEM) are presented in Figure 2.1 show that the NiSi nanowire growth on the Si substrate. Figure 2.2 show a typical Raman spectrum of NiSi nanowires. The main peaks of NiSi were detected at  $200\text{cm}^{-1}$  and minor peaks at  $294.5$  and  $362\text{ cm}^{-1}$  (J. Kim & Anderson, 2005).

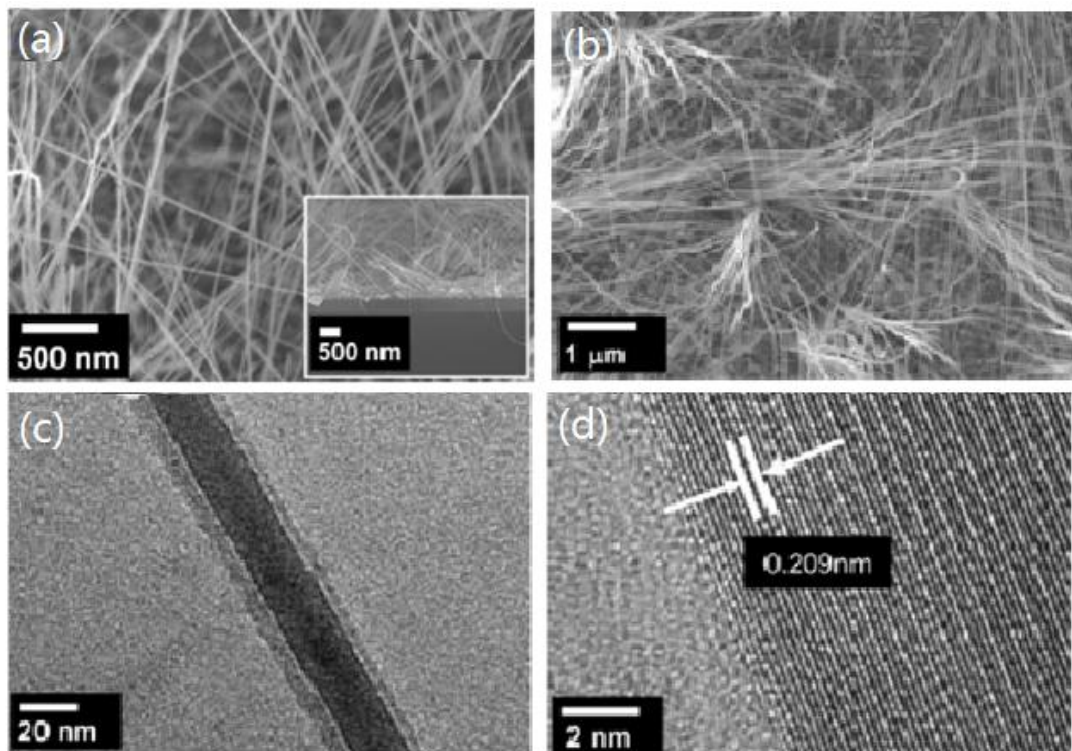


**Fig. 2.1** (a)~(b) SEM and (c)~(d) TEM image of NiSi nanowire growth by MIG (J. Kim, 2010).

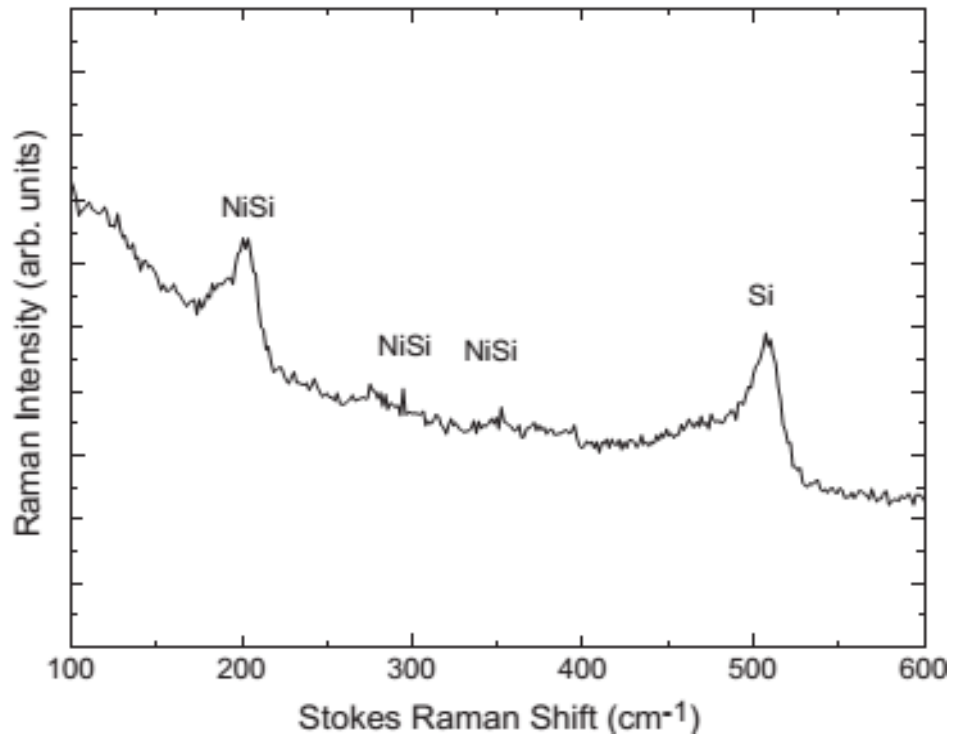


**Fig. 2.2** Raman spectrum of the NiSi nanowires (J. Kim & Anderson, 2005).

Silicon carbide (SiC) is a wide band gap semiconductor. It has some amazing characteristic, such as high saturation drift velocity, high breakdown field strength, and high thermal conductivity (V Schmidt, Wittemann, & Gosele, 2010; B. Wang et al., 2014). For silicon carbide, due to those aforementioned superior physical properties (Kolasinski, 2006), thus producing a semiconductor material with superior advantageous in (Hibino, Tanabe, Mizuno, & Kageshima, 2012; Kolasinski, 2006). Furthermore, crystalline cubic-SiC nanowires are frequently being adapted due to its high electron mobility (Bhatnagar & Baliga, 1993; Pallecchi et al., 2014) that enable its used in high-power, high temperature, and high-frequency electronic devices is widely used wide band gap semiconductor material. SiC nanowires also showed good field emission properties (Fissel, Schröter, & Richter, 1995).

Many techniques have been developed to synthesize SiC nanorods or nanowires.

Dai et al. (Dai, Wong, Lu, Fan, & Lieber, 1995) were the first to synthesis SiC nanorods and succeeded in 1995 through the reaction of carbon nanotubes with SiO or Si + I<sub>2</sub>. H-SiC nanorods was synthesis by Meng et al. (Meng, 1998) using carbothermal reduction reaction, and SiC nanowires was fabricated using the hot filament CVD method by Zhou et al. (Zhou et al., 1999). Li et al. (Y. Li et al., 2001) synthesized SiC nanowires by using silicon carbide rod as the anode arc discharge lately. There are some difficulties during the course of the reaction, to synthesize the SiC nanorods and nanowires on a Si substrate directly, since these methods use a variety of reactants, and the reaction requires high temperatures (typically greater than 1200°C). SiC nanowires were synthesized at low temperatures with high pressure by some groups (Lu et al., 1999). There are also reports on synthesis of SiC nanowires using metal as a catalyst (Honda et al., 2003; Liang, Meng, Zhang, Wu, & Cui, 2000). An example of SEM image of the SiC nanowires grown on a SiC thin film is shown in Figure 2.3 (He et al., 2013).

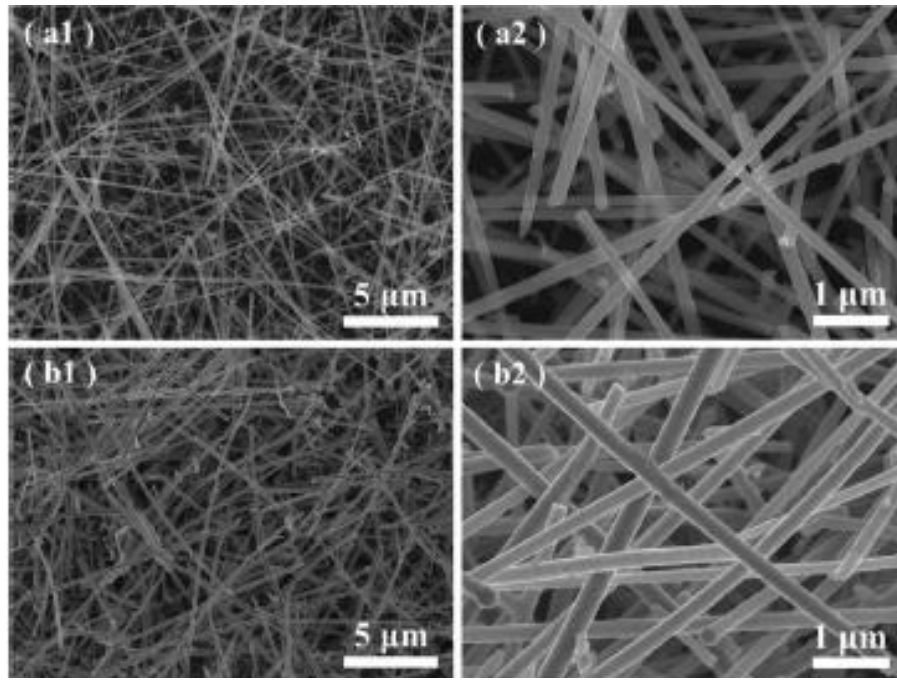
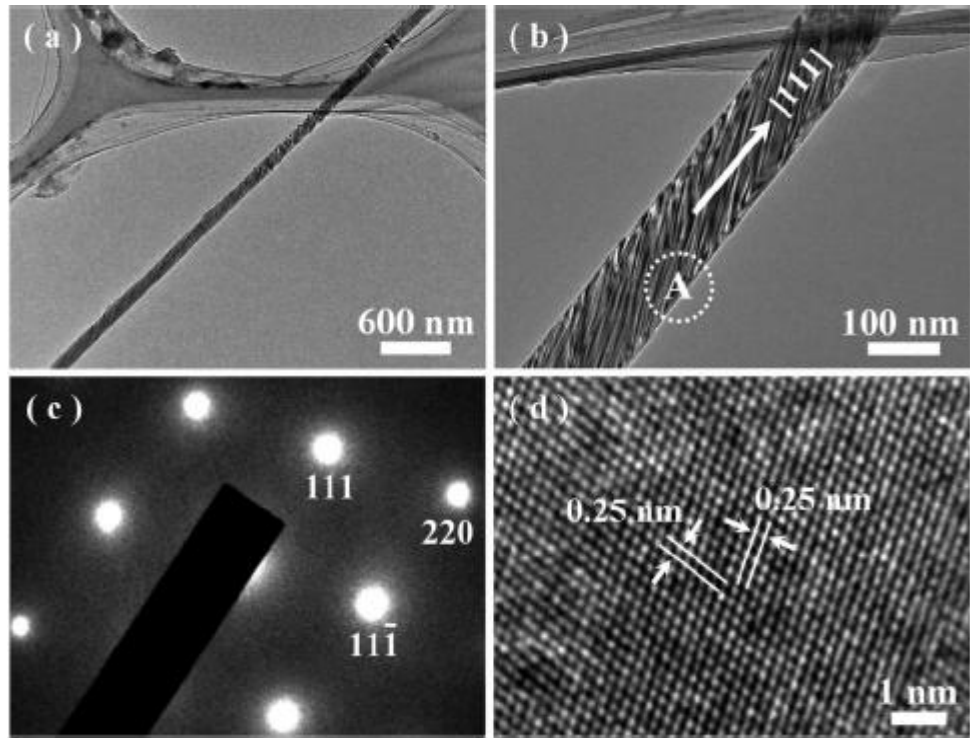


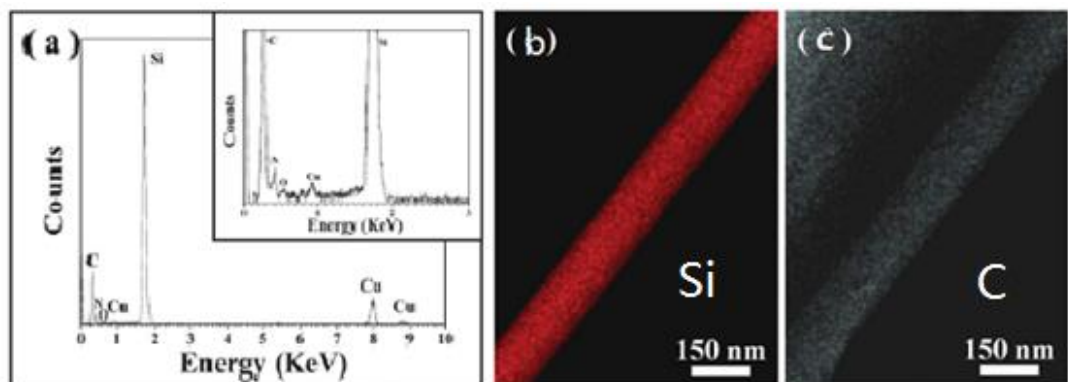
Fig. 2.3 Typical SEM images of SiC nanowires (He et al., 2013).

Typical TEM images of the nanowires show in Fig. 2.4(a) and (b). The nanowire is uniform in diameter along the entire length about 100 nm and showed the nanowires grow along the (R. Yan et al., 2009) direction. Fig. 2.4(c) is the corresponding selected area electron diffraction (SAED) pattern recorded from the marked area of A of the single nanowire, which can be indexed to the 3C-SiC [JCPDS Card No.29-1129]. The SAED pattern is identical over the entire nanowire, indicating that the nanowire is single crystalline. Fig. 2.4(d) presents the corresponding HRTEM image. Where the inter-planar spacing of two neighboring lattice fringes is  $\sim 0.25$  nm, and its well fitted to the [111] plane of 3C-SiC.



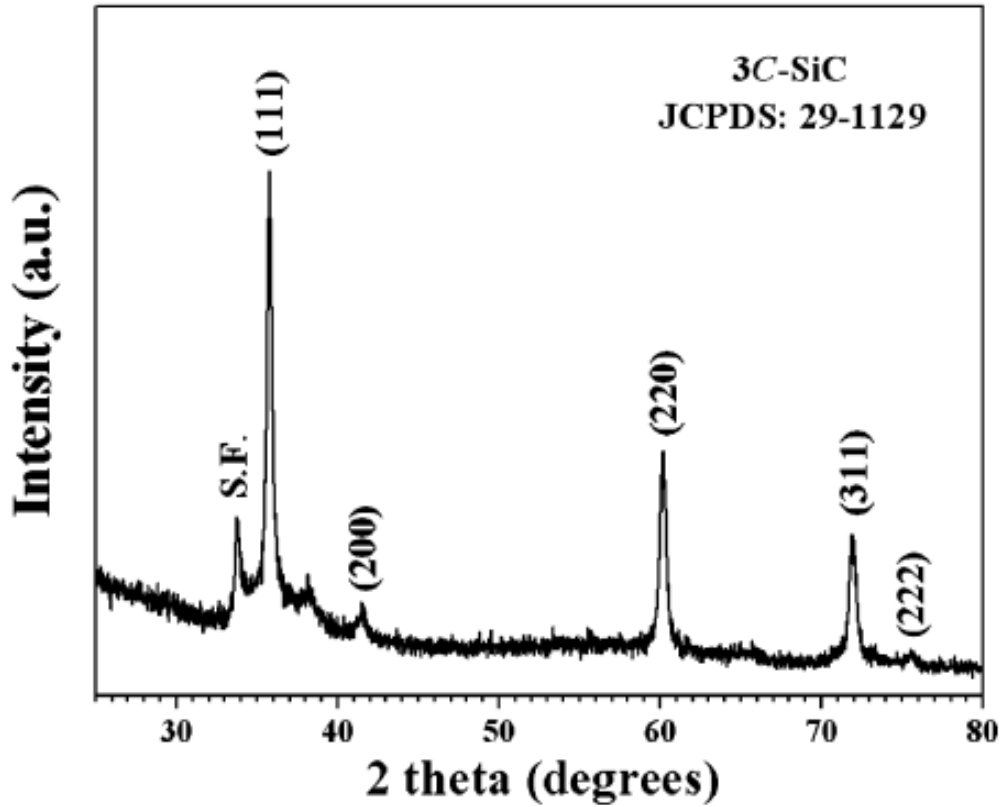
**Fig. 2.4** (a)~(b) Typical TEM images of a single SiC nanowire. (c)~(d) corresponding SAED pattern and HRTEM image of the SiC nanowire (He et al., 2013).

Fig. 2.5(a) shows a typical EDS spectrum recorded from the SiC nanowires, revealing that the nanowires mainly consist of Si, C and N, as well as a small amount of O. The O is from the amorphous  $\text{SiO}_x$  outer layer around the SiC wires, and the Cu comes from the copper grid used to support the TEM sample.



**Fig. 2.5** (a) A typical EDS spectrum of SiC nanowires. The inset is an enlarged spectrum. (b)~(c) The element maps of Si and C of a single nanowire (He et al., 2013).

The typical XRD pattern of SiC nanowires are presented in Figure 2.6. All diffraction peaks are in good agreement with JCPDS 29-1129. The lattice parameters of the nanowires can be calculated from the diffraction patterns.



**Fig. 2.6** XRD pattern of SiC nanowires (JCPDS 29-1129).

The room temperature Raman spectrum of the SiC nanowires is shown in Fig. 2.7. Two peaks at frequency of 794 and 968  $\text{cm}^{-1}$  are observed in the original Raman result. The bulk  $\beta$ -SiC crystal usually has two optical phonon modes: A transverse optical (TO) mode at 796  $\text{cm}^{-1}$  and a longitudinal optical (LO) mode at 972  $\text{cm}^{-1}$  (Z. Feng, Mascarenhas, Choyke, & Powell, 1988). On the other hand, the two peaks at frequency of 794 and 968  $\text{cm}^{-1}$  belong to the TO and LO modes of  $\beta$ -SiC respectively. For emergence of large red shifts of TO and LO phonon peaks in the nanowires, the abundant structure defects exhibit a significant effect and quantum confinement effect



acts like a minor part (Borowiak-Palen et al., 2005; Z. Li et al., 2003; S.-L. Zhang et al., 1999; Zou et al., 2006).

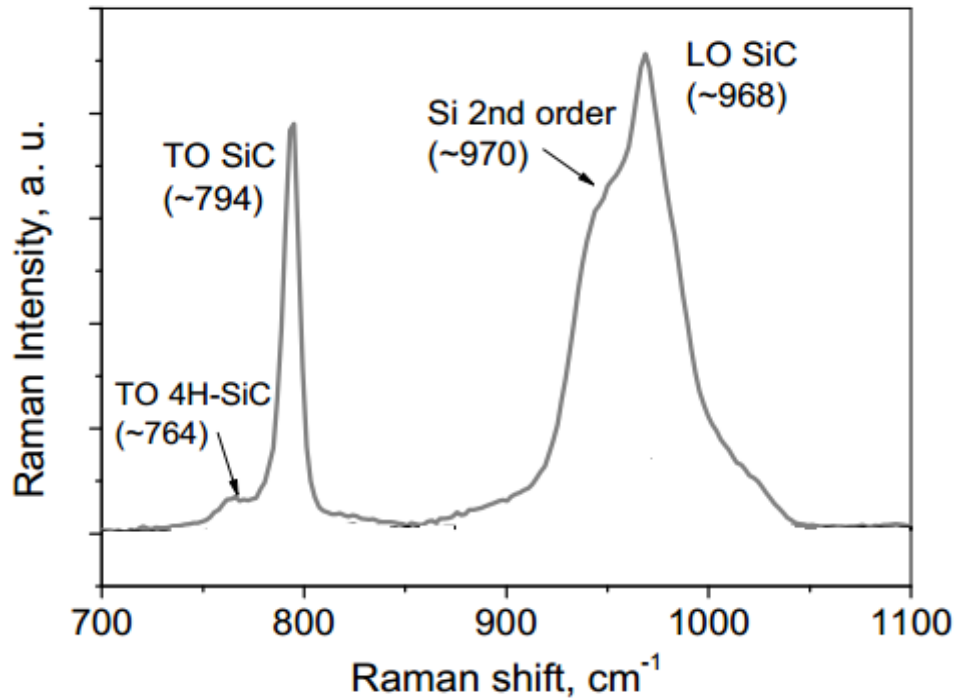


**Fig. 2.7** Raman spectrum of the SiC nanowires (Zou et al., 2006).

The spatial orientation of the assembly for two or more nanostructure assembly preferably is a combination having a different function. Because of the advances, they can generate performance independent single-component material, which is highly demanded. Engineering mixed multi-component nanostructures synthesis technology has attracted many interest, at our disposal assembled nanocrystals have a very different characteristics. Semiconductor nanocrystals, for example, in such a manner, the hybrid structure may be combined according to the particular application of the metal.

### **2.3 Nanowire diode**

There has been steady progress in demonstrating electrical components made of nanowires, such as field effect transistors, electron field emitters, switches, sensors, etc. The surface of the nanostructures has crucial role in determining the electrical and optoelectronic properties of nanodevices. As the surface-to-volume ratio is very high, the surface states also play a key role on optical absorption, gas sensing, luminescence and other properties. Thus, nanoscale electronic devices have the potential to achieve higher sensitivity and faster response than bulk material(Das, Myoung, & Kar, 2011).

Nanodevice units made from those one-dimensional nanostructures (single nanostructures as well as bunch of nanostructures) have attracted substantial research interests because they provide a unique platform for fundamental investigations. In addition, they can also serve as the building blocks for more complicated nano-systems and microsystems.

### **2.4 Hot-wire Chemical Vapor Deposition (HWCVD)**

Low pressure chemical vapor deposition (LPCVD) method has widely been used to develop Si/SiC core-shell nanowires, (Choi, Yao, Cui, & Cho, 2011). However, this technique has some disadvantages that include lower deposition rates and it also needed high temperature usually above 600°C for the process. Pressure and temperature are two variables that control the deposition rate (Curley, McCormack, & Phipps). Other techniques such as hot-wire chemical vapor deposition (HWCVD) also can be used in producing Si/SiC core-shell nanowires.

HWCVD is an elegant low pressure deposition technique that base on thermal

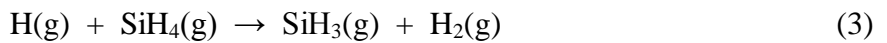
decomposition of precursor gases at the surface of resistively heated filament (usually Tungsten) to form radicals. These radicals adsorbed on the heated substrate (J. C. Lee et al., 2002).

Due to the lower production cost and large scale production capability, for the moment HWCVD has become a preferred-technique for the fabrication of Si/SiC core-shell nanowires. As a result making this method is getting attractive especially for industrial applications. It is also proven that this technique enhance the growth rate of Si nanowires besides having the advantages of low-temperature growth processes. Moreover, HWCVD is comparatively a better technique for the growth of Si/SiC core-shell nanowires since it provides an ion-free deposition by catalytic decomposition of the source gas using a catalyzer usually tungsten.

HWCVD was proposed in 1979 by Wiesmann (Wiesmann, Ghosh, McMahon, & Strongin, 1979) in the preparation of highly hydrogenated amorphous silicon (a-Si:H) film, but the electrical properties of hydrogenated amorphous silicon was inferior to the film prepared by plasma-enhanced chemical vapor deposition (PECVD). Due to this reason, this technique has been neglected until after 1985 Matsumura et al prepared excellent fluorinated amorphous silicon by the use of this technique (Matsumura & Tachibana, 1985). Because they believe the deposition process, the hot tungsten filament act as a catalyst, then this process is called catalytic chemical vapor deposition (catalytic CVD). Doyel, who after three years under similar conditions to prepare a good quality hydrogenated amorphous silicon, they call the evaporation surface decomposition (evaporative surface decomposition), because they think the hot-wire decompose air source into primitives that was used in the deposition (Doyle et al., 1988).

1991 Mahan prepared device-level quality by hot-wire having, the hydrogen content only 1 % of a-Si: H and compare the different with PECVD and HWCVD, because suspect the catalytic reaction with hydrogen and hot-wire, he re-name this process hot filament assisted chemical vapor deposition, which sparked a passion to HWCVD study (Mahan, Carapella, Nelson, Crandall, & Balberg, 1991).

Silane pyrolysis has been used as silicon source for numerous of decades. Although the deposition surface temperature was low than the filament temperature ( $T_f$ ), but it is a surface pyrolysis process (R Robertson, Hils, & Gallagher, 1984; Robert Robertson & Gallagher, 1986). Before prepared a-Si:H, HWCVD is also used to prepare diamond by pyrolysis mixture  $\text{CH}_4/\text{H}_2$ . However, in the preparation of the diamond the pressure is far low than preparation of the silicon based device, which makes the kind of filament and atmosphere around the filament is not important to the growth diamond. In contrast, silicon-based nano-wire is prepared mainly under low pressure, there are one or two times reactive before deposition, thus making a kind of excitation from the filament important (Doyle et al., 1988). The relations below present the decomposition mechanism of  $\text{SiH}_4$  gas in the HWCVD:



This corresponding deposition process is shown in Figure 2.8.

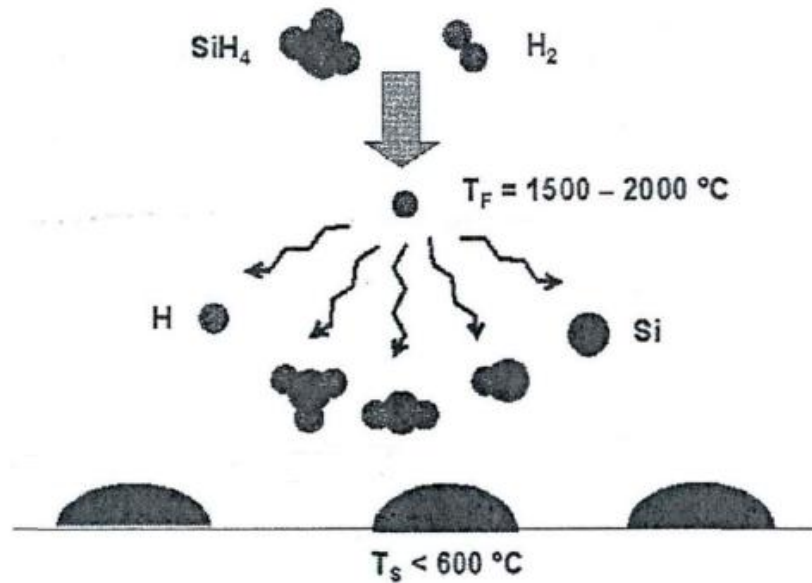
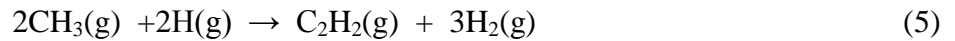
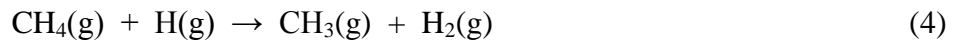


**Fig. 2.8**  $\text{SiH}_4$  deposit process of hot-wire chemical vapor deposition (Doyle et al., 1988).

Doyle team studied  $\text{SiH}_4$  decomposition efficiency tungsten surface and the relationship with kinds of primitive and hot filament temperature (Matsumura, 1986) It was found that at lower pressure, when.  $T_f > 1800^\circ\text{C}$ , the probability of reaction of the silane is relatively high, then the primitives of thermal decomposition silane mainly four H atoms and one Si atoms. At higher temperatures, H atoms can be more quickly escape from the hot filament surface. For this case, the high energy of hot-wire, there are high probability of reaction with silane and tungsten surface dangling bond, and decomposed into Si and H atoms. The decrease of the hot filament temperature below  $1800^\circ\text{C}$ , tungsten surface dangling bonds are occupied by H, a silane and tungsten surface dangling bonds reduce the probability of reaction, so that the silane can not be combined with the tungsten surface (Matsumura, 1986). The energy of H decomposition is low, so just H primitive come out when  $T_f$  further reduced to  $1500^\circ\text{C}$ , the release of Si primitives becomes negligible, almost all of the silane are decomposed Si and W are

a bond and W into the lattice structure of the compound becomes. Surprisingly, when the tungsten wire temperature below 1300°C, still H atoms are released.

The tungsten surface also has a significant effect on decomposition efficiency of CH<sub>4</sub>. Fig. 2.9 shows the effect of filament temperature to the concentration of H, CH<sub>4</sub>, CH<sub>3</sub> and C<sub>2</sub>H<sub>2</sub> above substrate. The relations below demonstrate the decomposition mechanism of CH<sub>4</sub> gas during the hot-filament processes:



Hydrogen atomic concentration increases monotonically with the filament temperature. When the temperature is lower than 1700°C, methane decomposes very slowly. The filament temperature rise to above 1773°C substantial decomposition of CH<sub>3</sub>. However, the high temperature generates stable acetylene by methane decomposition. Molecular hydrogen cracking around 1973°C significantly accelerated the rate of atomic hydrogen generation. Further increase the filament temperature around 2273°C, atomic hydrogen generation rate slow down. Fig. 2.9(b) use infrared absorption intensities of CH<sub>4</sub> and C<sub>2</sub>H<sub>2</sub> to characterize the rate of methane decomposition (Jafari, Akbarnejad, Ghoranneviss, Yazdi, & Rezaei, 2015; Jing-Biao, Yu-Rong, & Rong-Chuan, 1996; QI, CHANG, CHEN, WANG, & LIAO, 2003).

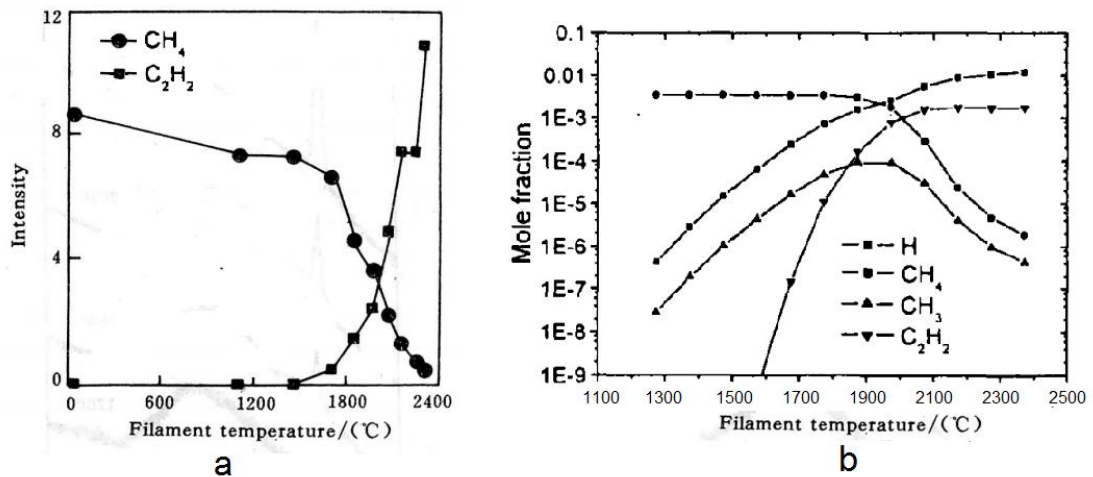


**Fig. 2.9** (a) Mode fraction and (b) infrared absorption intensities of C<sub>2</sub>H<sub>2</sub> and CH<sub>4</sub> as a function of filament temperature (Jing-Biao et al., 1996; QI et al., 2003).

## 2.5 Nanowire grow mechanism

There are several growth mechanism of nanowires were reported, such as gas-liquid-solid (VLS), solid-liquid-solid (SLS), and solid-solid (SS) type.

The VLS model that was firstly proposed by Wagner and Treuting, still greatly adopted until today in growing nanowires (Edwards & Happel Jr, 1962; Wagner & Ellis, 1964). As for absorbing liquid catalyst gas-phase reactants (Morales & Lieber, 1998) strongly favored spots. the number of possible catalyst materials are quite large (Table 1). Although the quality of the wires obtained as well as the required growth conditions differ strongly, there are also similarities in the behavior of the different catalysts. I will adopt the classification scheme similarly introduced by Bootsma et al. (Yiying Wu & Yang, 2001). The catalyst materials are classified into three different categories: typeA, type-B, and type-C, as shown in Figure 2.10(a). Type-A catalysts are the Au-like metals. Their phase diagram is of the simple eutectic type; that is, it is dominated by a single eutectic point. Type-B catalysts are the low Si solubility metals. Their phase diagrams

also show a single dominant eutectic point but no silicide phases. Type-C catalysts are the silicide forming metals. Their phase diagram indicates the presence of one or more silicide phases.

In addition, the lowest eutectic temperature is higher than 800°C. Typical type-C catalysts are Ni, Pt, or Ti. Fig 2.10(b) show minimum temperatures of certain metals required for vapor-liquid-solid (VLS) growth of Si nanowires plotted versus their respective impurity level energies in Si. The energies of these impurity levels are given on the rhs with respect to the middle of the band gap (assuming a band gap of Si of 1.12 eV). The color code refers to the catalyst classification of Figure 2.10: red, type-A; orange, type-B; blue, type-C.



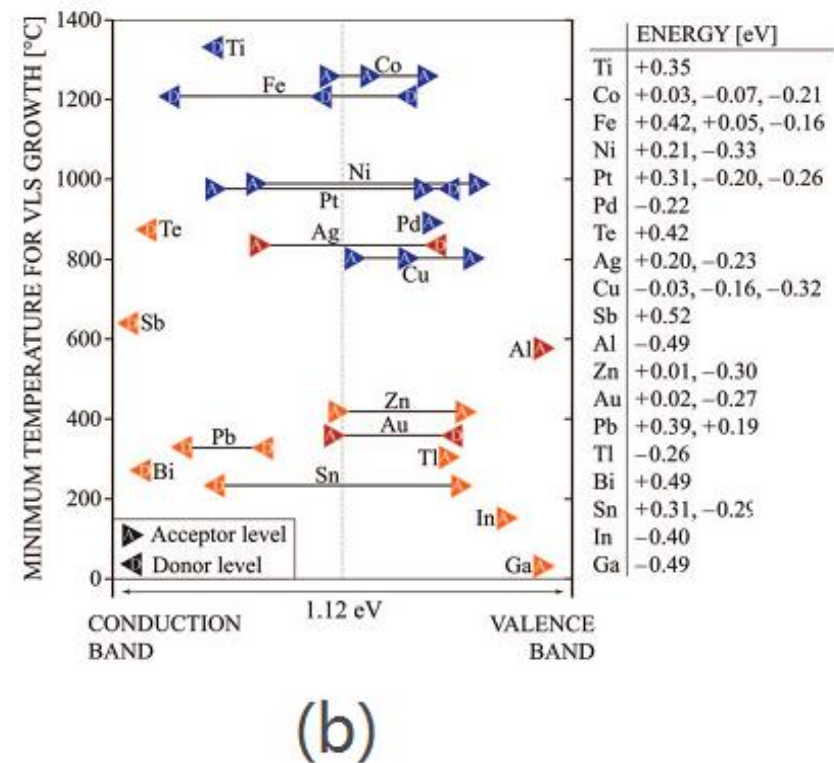
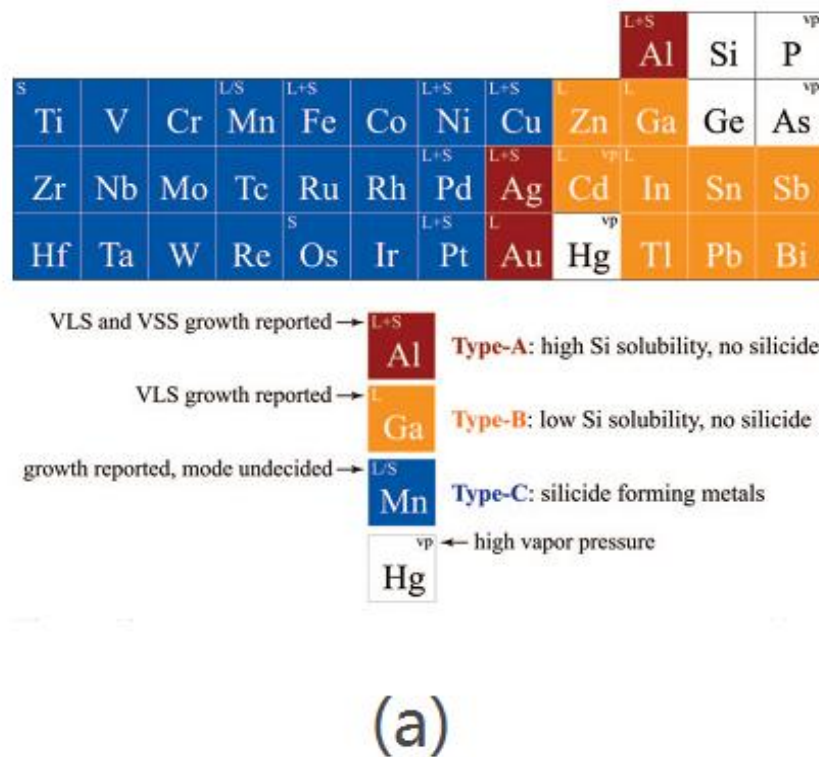


**Fig. 2.10** (a) Periodic table with potential catalyst metals classified according to their phase diagram. (b) Minimum temperatures of certain metals required for vapor-liquid-solid (VLS) growth of Si nanowires (V. Schmidt, Wittemann, & Gösele, 2010).

TABLE 1. Nanowire fabrication types and conditions

<b>Growth type</b>	<b>Catalyst</b>	<b>Gas type Si source</b>	<b>Temperature (°C)</b>	<b>Reference(s)</b>
VLS	Au	Yes	300–600	(Cui, Lauhon, Gudiksen, Wang, & Lieber, 2001; Westwater, Gosain, Tomiya, Usui, & Ruda, 1997; Yue Wu, Cui, et al., 2004; Zeng et al., 2003)
VLS	Fe	No	1150-1200	(S. Feng, Yu, Zhang, Bai, & Ding, 2000; N. Wang et al., 1999; D. Yu et al., 1998; H. Zhang et al., 1998)
SLS	Ni	No	950	(Xihong Chen, Xing, Xu, Xiang, & Yu, 2003; H. Yan et al., 2000)
SS	Ni	Yes	1050	(K.-H. Lee et al., 2004)
MIG	Ni	No	575	(J. Kim & Anderson, 2005)
MDG	Ni	Yes	320–420	(J. Kim & Anderson, 2005)

Numerous studies had reported nanowire can be grown in the temperature range of 320-600°C by using gas type silicon source such as silicon tetrachloride or SiH<sub>4</sub> with the presence of Au as catalyst (Cui et al., 2001; Westwater et al., 1997; Yue Wu, Cui, et al., 2004; Zeng et al., 2003). Fig. 2.11 shows schematic diagram of VLS growth mechanism. At first the vapor phases of Si-H would react with the used catalysts of Au, leading to the formation of molten Au alloy catalytic droplets (schematically shown as step I in Fig. 2.11). With the increase of the temperature, the vapor species would dissolve in the formed catalyst liquid droplets, thus leading to the nucleation of Si nanowires (schematically shown as step II in Fig. 2.11). At the beginning of the growth of Si crystals, the small size of the nuclei, compared to the large catalyst droplet, would result in a large contact angle between the nuclei and catalytic droplet, which generates an outward force (F) on the nanostructure (shown as the marked area of V in Fig. 2.11).

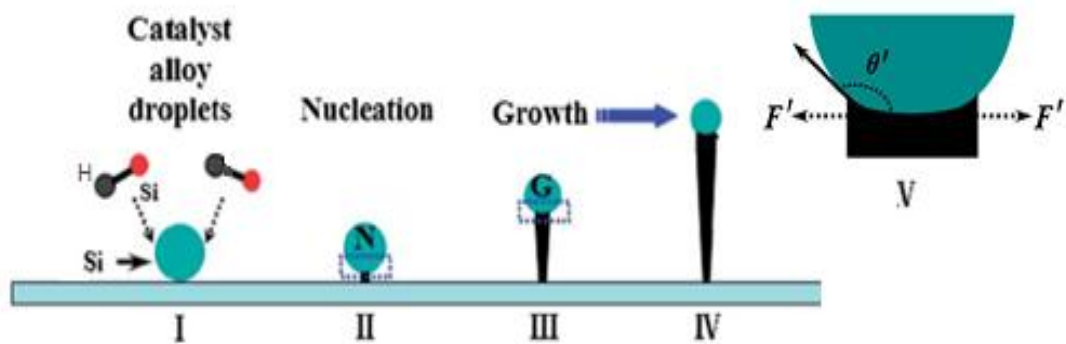


**Fig. 2.11** Schematic illustration for the growth of nanowires with on the VLS mechanism (Cui et al., 2001).

Otherwise, the high temperature near or above 1000°C is necessary to liquefy the catalyst and the Si (S. Feng et al., 2000; N. Wang et al., 1999; D. Yu et al., 1998; H. Zhang et al., 1998). Recently, SLS synthesis using metal catalyst coated Si prevents

direct evaporation of Si atoms, but the results in the formation of droplets of silicon and metal, even under high temperature 900-950°C (Xihong Chen et al., 2003; H. Yan et al., 2000). It is also claimed that SS synthesized in 1050°C by simple heat treatment in the growth of nanowires CH<sub>4</sub>: H<sub>2</sub> gas mixture. In this mechanism, at the tip of the nanowire, the SLS mechanism has been observed different metal particles (K.-H. Lee et al., 2004).

Unique growth mechanism of nanowires, metal induced growth (MIG) methods grown highly linear of NiSi nanowires by the solid phase reactions at 575°C (J. Kim & Anderson, 2005). Low temperature treatment is ideal for application as a nanowire interconnected with the structure of the manufactured nanoscale little or no damage. Summary of nanowire growth type and the processing temperature are shown in Table 1. In this report, the surface morphology was observed by a variety of metal catalysts, and the MIG growth nanowire have been reported with different Ni silicide (nickel silicide, Ni<sub>2</sub>Si and Ni<sub>3</sub>Si<sub>2</sub>) present on the nanowires. These nanowires grown on Ni decomposition Ni film from the inside surface temperature range of 320-420°C SiO<sub>2</sub> coated Si wafer (10-100 nm) through the silane gas (J. Kim, 2010).

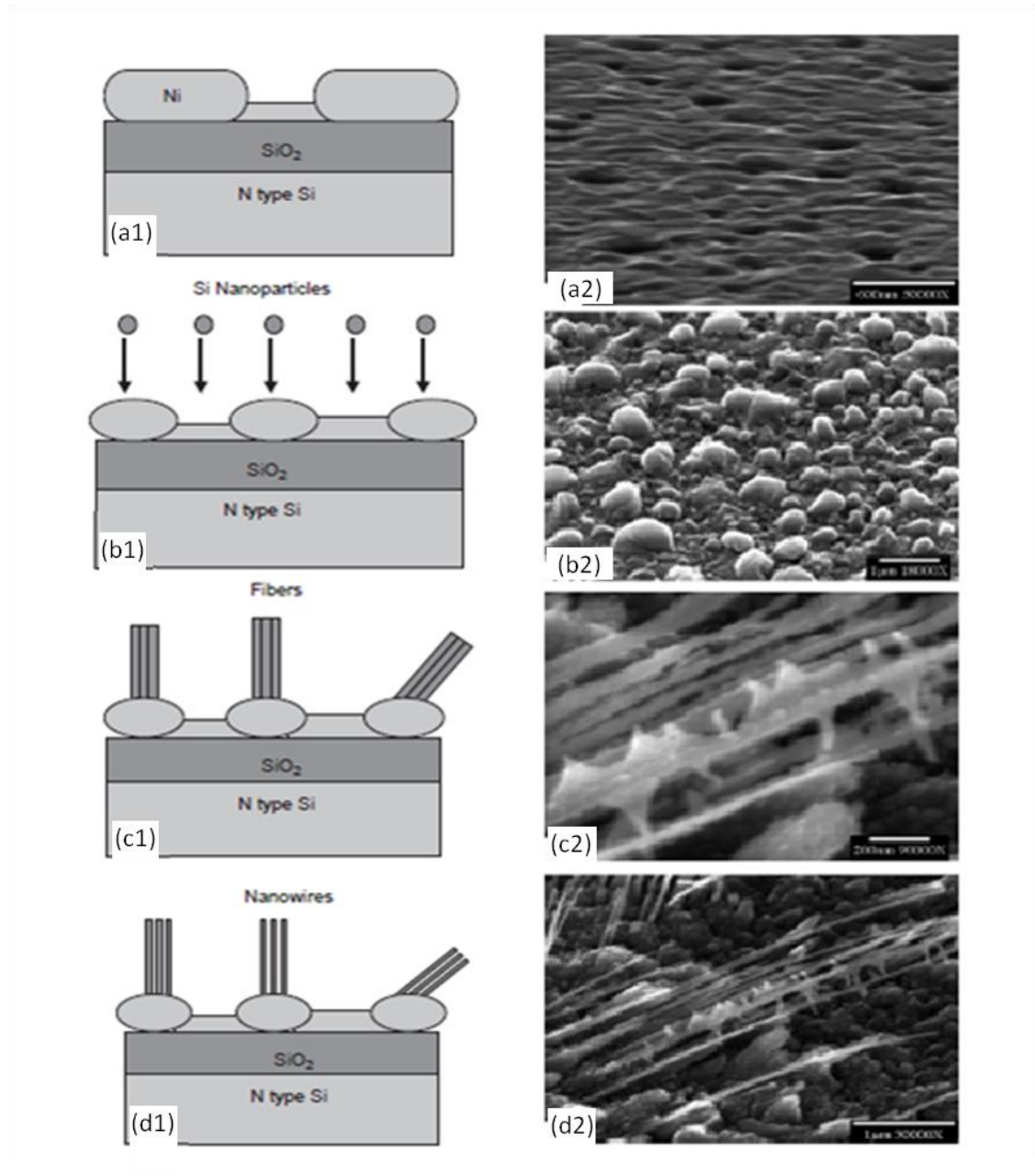


**Fig. 2.12** Schematic diagram and SEM image of MIG nanowire growth. (a) Groove and agglomeration of Ni layer by heating, (b) Clustering during Si supply, (c) Formation of nanofibers, and (d) Growth of nanowires (J. Kim & Anderson, 2005).

## CHAPTER 3

### METHODOLOGY

#### 3.1 Introduction

This chapter is organized mainly into 3 sections. The first section describes the HWCVD system that used for synthesis of the nanowires. Section 3.2 explains the experimental techniques for substrate cleaning and deposition procedures. The last section discusses the characterization technique used in this work.

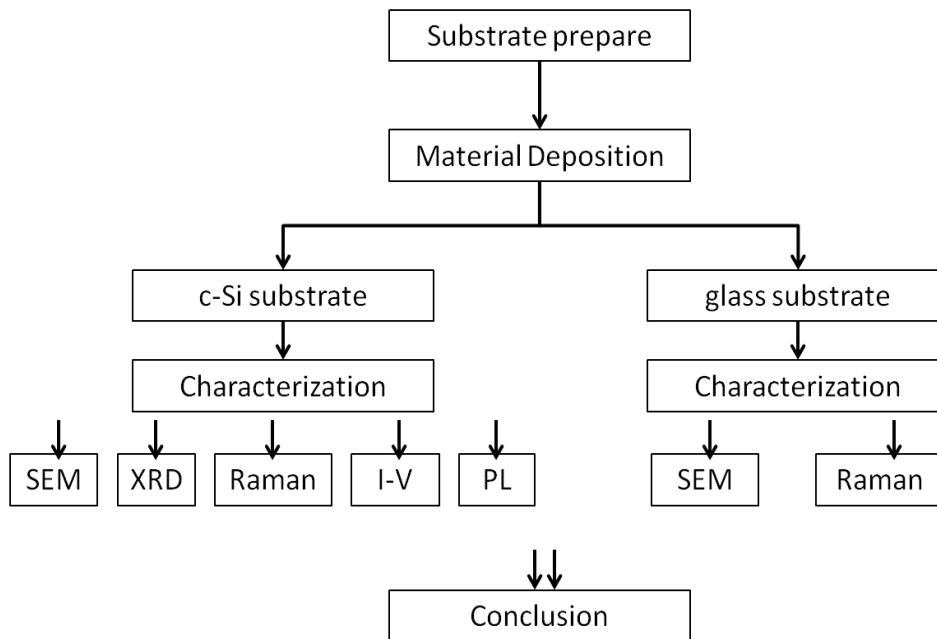


**Fig. 3.1** Flow chart of this work.

#### 3.2 Hot-Wire Chemical Vapor Deposition

Most of the samples in this thesis were synthesis in the home-built HWCVD system with the schematic diagram as illustrated in Figure 3.2(a). The system consists

of six parts; the vacuum chamber, plasma generator, hot-wire power supply, vacuum pump, valve, gas line management and substrate heating elements.

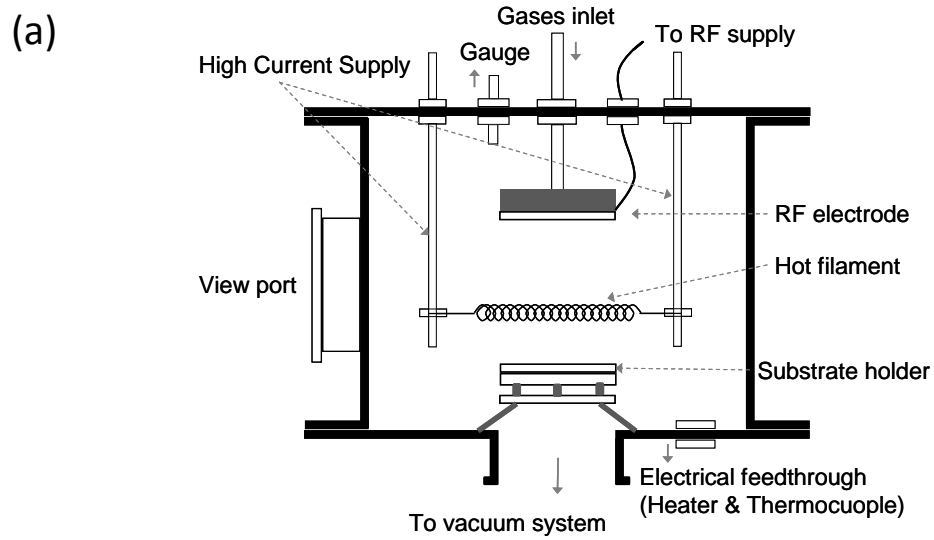


**Fig. 3.2** (a) Schematic diagram of the HWCVD reaction chamber. (b) Real picture of the HWCVD vacuum system.

### 3.2.1 Vacuum chamber

This vacuum chamber for deposition made of cylindrical stainless steel show in Fig. 3.2(b). The vacuum chamber is well-sealed by using viton o-rings directly connected to a vacuum pump. The connecting tube has an air admittance valve for venting purposes. A glass viewport for viewing the interior of the reactor was attached on the body of the chamber. It also acts as a window for the optical pyrometer used to determine the filament temperature. A 2.5cm diameter stainless steel made substrate holder is designed to hold substrates. The heater rod and thermocouple are attached to the substrate holder which is grounded to the earth and isolated from the body of the reactor by quartz stands.

### 3.2.2 Plasma generator

Plasma generator (Fig. 3.3) is electrical equipment that employ apply high frequency (13.5MHz) power to produce plasma. A stainless steel electrode-cum-gas showerhead is installed inside vacuum chamber with the gas inlet tube and is placed at a distance of 5 cm from the substrate holder. The electrode is fabricated into cone-shaped holes. The inlet and outlet diameter of the hole is 2.2 mm and 1.0 mm, respectively, while the distance between holes is 1.0 cm. Precursor gas can be dispersed uniformly from these holes. The electrode is powered for plasma generation. It is connected to the RF generator via an impedance matching network. The plasma is generated between the powered electrode and grounded substrate holder by applying RF power. An impedance matching network is employed to match the load impedance of plasma to the impedance of the DC generator, so that the reflected power from plasma to RF generator can be



minimized.

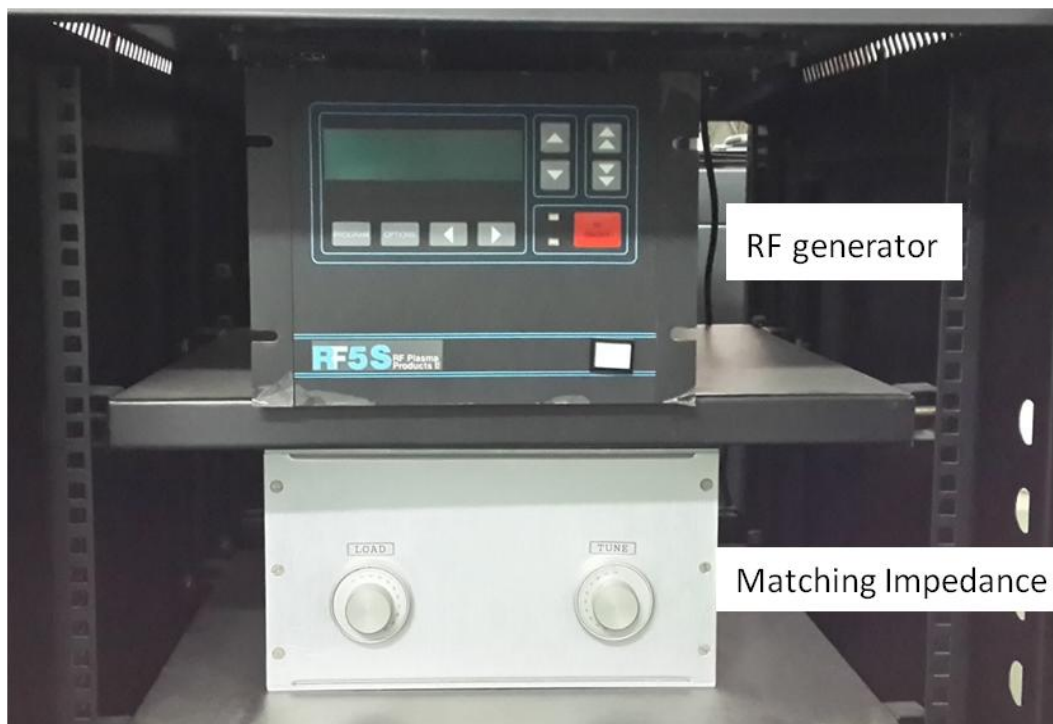


**Fig. 3.3** Photograph of RF generator used.

### 3.2.3 Hot-wire power supply

A tungsten wire (purity of 99.95 %) filament coil serves as a hot filament for evaporation of metal catalyst and decomposition of source gases. The tungsten filament is placed on a filament holder, which is connected to a power supply. The power supply consists of a voltage regulator (IBC voltage regulator 1P-1kVA) with voltage ranging from 0 – 250 V and a step down transformer. The transformer is used to step down the output voltage to a range of 0 – 20 V with a maximum current of 60 A. By regulating the voltage supplied to the tungsten filament, different filament temperatures (Fig. 3.4(b)).  $T_f$  can be controlled for deposition. An ammeter is connected with the voltage supply to measure the current flow through the tungsten filament.  $T_f$  is measured by a

pyrometer (Reytek, Raynger, 3i). The detector of the pyrometer is stimulated by the incoming infrared energy and produces a signal to the circuitry, which will process the signal and compute the  $T_f$ . The tungsten filament is pre-heated to remove surface contaminations such as carbon and other metallic elements before deposition. Pre-heat treatment is carried out for 10 minutes at  $T_f \sim 1600^\circ\text{C}$  in  $\text{H}_2$  with flow rate of 100 sccm.



**Fig. 3.4** Photograph of a process for (a) plasma treatment and (b) hot-wire decomposition of silane processes.

#### 3.2.4 Vacuum system

Vacuum pump is used to remove gas molecules from a sealed volume, that will subsequently leave behind a vacuum condition. A rotary pump volume of the container is enlarged. Continue vacuum chamber indefinitely without requiring infinite growth, a compartment vacuum can be repeatedly closed off, exhausted and expanded. The simplest is a circular rotary pump rotor rotating a larger circular internal cavity. Offset of the centre of these two circles, causing eccentricity. Leaves can be slid into and out of the rotor and seal all the edges to create a blade chamber is pumped to do the work. In

the suction side of the pump, increasing the volume of the vane chamber and filled with a pressure fluid inlet forced. In the discharge side of the pump, the decrease of the volume of the blade chambers, thereby forcing fluid out of the pump. Rotary vacuum pump can reach pressures as low as  $10^{-3}$  mbar.

### 3.2.5 Gas supply

Highly purified  $\text{SiH}_4$  (99.9995 %) and  $\text{CH}_4$  (99.999 %) are used as the precursor gas for deposition process.  $\text{H}_2$  gas with the purity of 99.999 % is used to dilute the  $\text{SiH}_4$  and  $\text{CH}_4$  gas during deposition. In addition to it,  $\text{H}_2$  gas also serves as a precursor in  $\text{H}_2$  plasma treatment and pre-heating of coiled tungsten filament process. Purified nitrogen ( $\text{N}_2$ ) gas (99.999 %) is mainly used for gas line cleaning, purging and  $\text{SiH}_4$  diluting in vacuum pump. The source gas tanks are stored in a gas room. The  $\text{SiH}_4$  gas tank is kept in a secured gas cabinet equipped with a control panel. The source gases are introduced into the vacuum chamber through the gas line (Fig. 3.5). A check valve is installed in each gas line to prevent the backflow of the source gas. The gas flow rate is accurately controlled by using a mass flow controller (MFC) with unit reading of sccm (standard cubic centimeters per minute). The  $\text{SiH}_4$  and  $\text{CH}_4$  gas flow rate are separately controlled by an AALBORG MFC in a flow rate range of 0–10 sccm.  $\text{H}_2$  gas flow rate can be varied from 0–100 sccm using an Aalborg Mass Flow Controller with its display meter. Figure 3.5 below shows the photograph of gas line in which it is use for the process of deposition. Gas use for deposition process is  $\text{SiH}_4$ ,  $\text{CH}_4$  and  $\text{H}_2$ .



**Fig. 3.5** Photograph of the gas line.

### 3.2.6 Heating supply

In order to prepare sample, relatively higher substrate temperature than those of film deposition are required to activate the metal catalyst or form a metal-Si alloy. Substrates are heated to 450°C. The heating element of the CVD system is constructed based on this temperature requirement. A Watlow Fire Rod SFMH80 A-4183 heater cartridge is employed for substrate heating (Fig. 3.6), which operates within temperature limit of 500°C. The heater cartridge is clamped in between of the substrate holder, so that heat can be transferred from the stainless steel substrate holder to the substrate. The temperature controller is connected to a thermocouple (Maltec-T type K thermocouple), installed at the bottom of the substrate in the vacuum chamber. The

thermocouple is used to directly measure the temperature of the substrate.

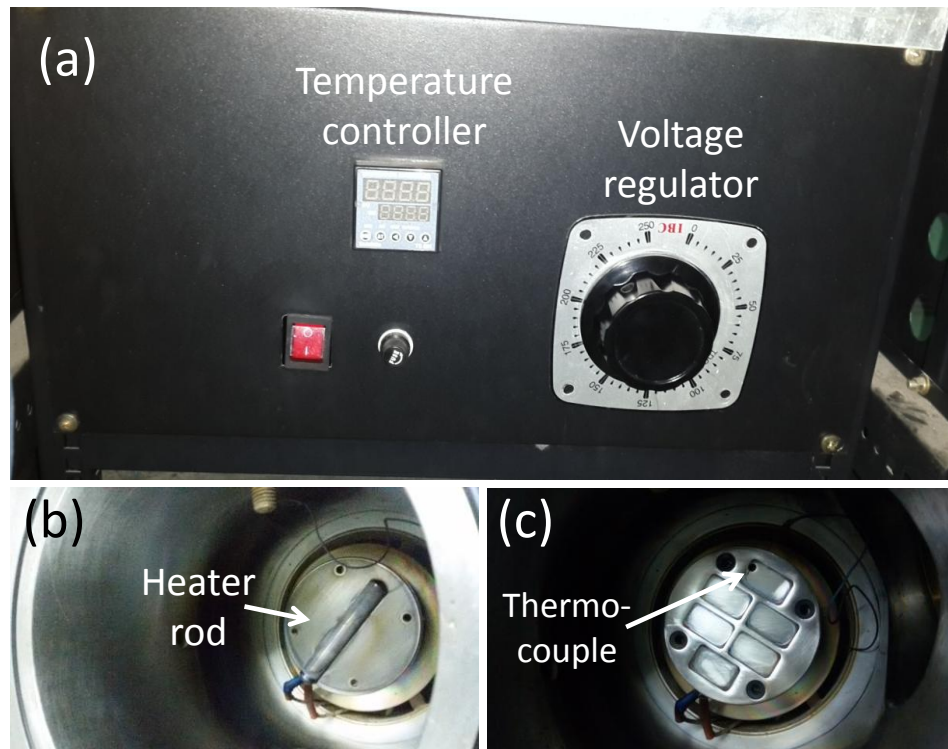


**Fig. 3.6** Real pictures of (a) Temperature controller and voltage regulator panels, (b) heater rod and (c) Thermocouple.

### 3.3 Experiment Method

Experiment method includes 4 steps. First clean c-Si and glass substrates. Then The tungsten filament need be pre-heated to remove surface contaminations. The 3rd step is deposited on the surface of substrates. At the last grow nanowires by HWCVD system.

#### 3.3.1 Substrates cleaning

The c-Si and glass substrates were cleaned repeatedly by following the RCA-I and II cleaning procedures before it is being introduced into the reactor (Kern, 1970). The solvents involved hydrochloric acid (37 % HCl,  $M = 36.49$  g/mol, diluted in  $H_2O_2$  and

deionized (DI) water in a ratio of 1:1:6), ammonia (25 %  $\text{NH}_4\text{OH}$ ,  $M = 17.03 \text{ g/mol}$ , diluted in  $\text{H}_2\text{O}_2$  and DI water in a ratio of 1:1:5).  $\text{HCl}$  can be used to remove residual metal contaminations, such as Al, Mg and Zn.  $\text{NH}_4\text{OH}$  can be used to remove organic contaminations and dissolved metal (Au, Ag, Cu, Ni, Cd, Co and Cr) contaminations.

Glass substrates were cleaned using decon 90, acetone ( $\text{C}_3\text{H}_6\text{O}$ ,  $M = 58.08 \text{ g/mol}$ ), ethanol ( $\text{C}_2\text{H}_5\text{OH}$ ,  $M = 46.07 \text{ g/mol}$ ). The glass substrates were immersed in a beaker containing decon 90 solution and sonicated in ultrasonic bath for 20 minutes to remove oil and gross dirt contaminations. This was followed by rinsing in acetone; ethanol and DI water subsequently to remove organic impurities such as the hydrocarbon dried by  $\text{N}_2$  purging.

### 3.3.2 Pre-heating filament

The tungsten filament (Fig. 3.7 (a)) is pre-heated to remove surface contaminations such as carbon and other metallic elements before deposition. The pre-heat treatment is carried out for 10 minutes at  $T_f \sim 1600^\circ\text{C}$  in  $\text{H}_2$  with flow rate of 100 sccm. Both for Ni evaporation and deposition process required a pre-heated tungsten filament. Fig. 3.7(b) shows the setup of the filament which is hold by the filament electrode.



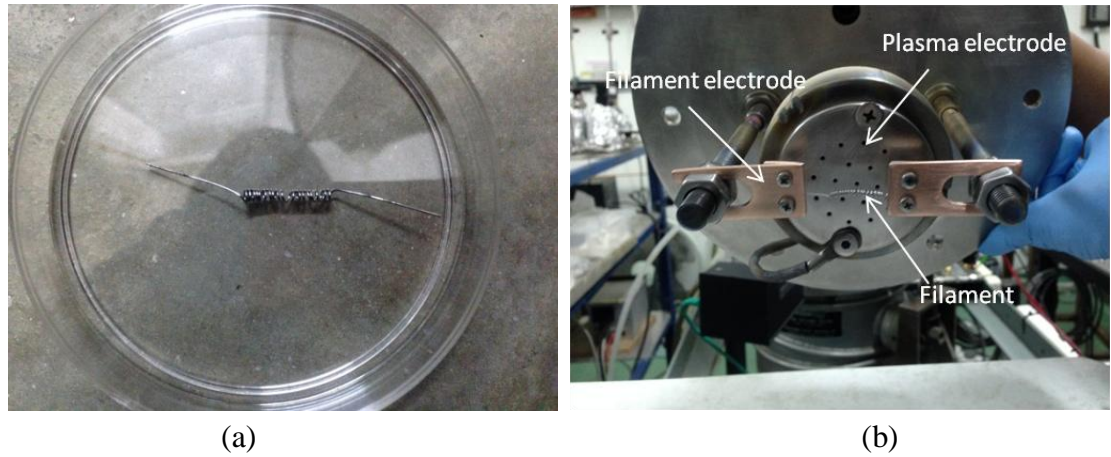
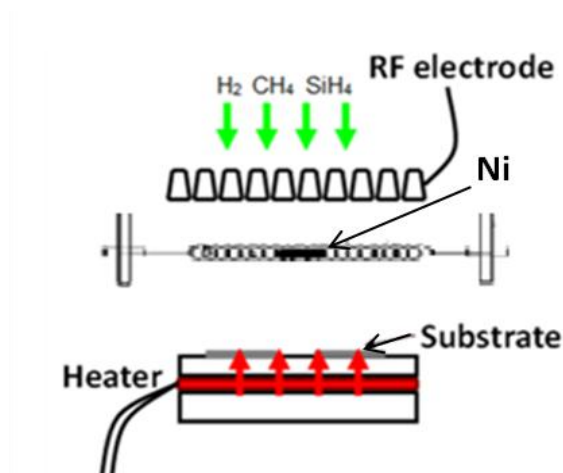


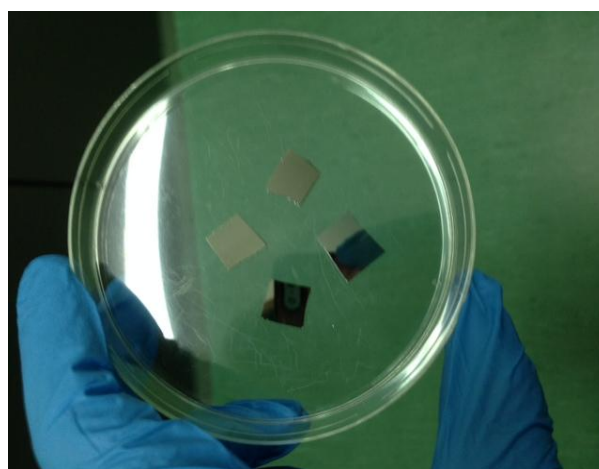
**Fig. 3.7** (a) Photograph of tungsten Filament. (b) Photograph of setup of filament for nickel evaporation and deposition processes. Filament is placed in a filament electrode.

### 3.3.3 Ni evaporation

At the beginning a layer of nickel about 40 nm was deposited on the substrates. Nickel was used as a catalyst to induce the growth of the nanowires. A 1 mm x 6 mm nickel (purity of 99.999 %) was used as the source of evaporation. The nickel piece was tightly hung onto the coiled filament. The evaporation was carried out at filament temperature about 1600°C for 5 min with H<sub>2</sub> flow rate of 100 sccm. Figure 3.8 (a) shows the substrate holder where all the substrate is place for Ni evaporation process while Figure 3.8 (b) shows the Ni coated on glass substrates.



(a)



(b)

**Fig. 3.8** (a) Schematic diagram of Ni evaporation process. (b) Photograph of the Ni coated on glass substrates.

### 3.3.4 Deposition

Nanowires were prepared on Ni coated substrates by a home-built HWCVD system. The Ni film thickness about  $40 \pm 5$  nm was deposited on the heated substrates in a vacuum condition. Prior to deposition, the Ni films were treated by atomic hydrogen plasma for 10 minutes (Fig. 3.9a). The substrate temperature, pressure, hydrogen flow-rate and radio-frequency (RF) power for plasma treatment were fixed at  $450^\circ\text{C}$ , 0.75 mbar, 100 sccm and 5 W respectively. During the deposition, the filament



temperature varied from 1100 to 1950°C, respectively. The filament temperature was measured using a pyrometer model Reytek, Raynger 3i. The filament to substrate distance was fixed at 2 cm. The SiH<sub>4</sub>, CH<sub>4</sub> and H<sub>2</sub> flow-rates were fixed at 1, 2 and 100 sccm, respectively (Fig. 3.9b). The deposition temperature was remained at 450°C and the deposition pressure was increased to 3 mbar and kept at 3 mbar for the whole deposition process (TABLE 2).

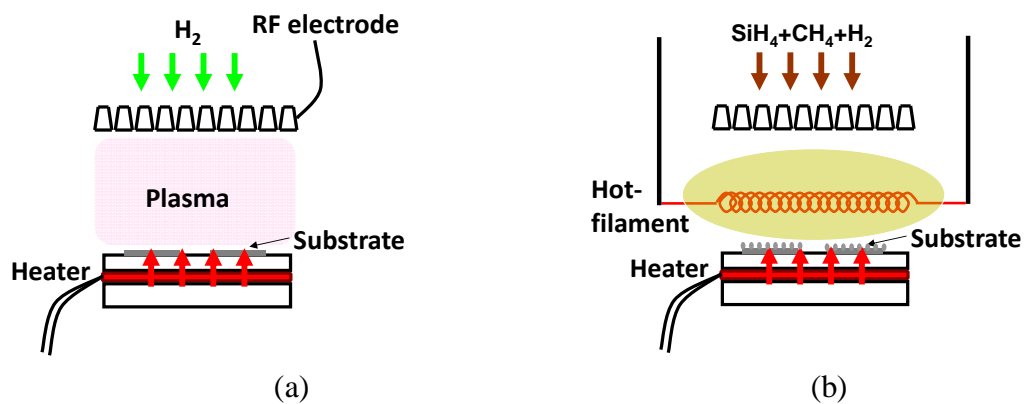


**Fig. 3.9** (a) Plasma treatment process to form Ni nano-island (b) Decomposition of gas precursors (SiH<sub>4</sub>, CH<sub>4</sub>, H<sub>2</sub>) during deposition process.

TABLE 2: Deposit parameters in this work.

Parameter	Value	
Substrate type	c-Si	glass
Deposition pressure	3 mbar	3 mbar
Substrate temperature	450 °C	450 °C
Filament temperature	1000 ~ 1900°C	1000 ~ 1900°C
Silane (SiH <sub>4</sub> ) flow-rate	1 sccm	1 sccm
Methane (CH <sub>4</sub> ) flow-rate	2 sccm	2 sccm
Hydrogen (H <sub>2</sub> ) flow-rate	100 sccm	100 sccm
Deposition time	5 minutes	5 minutes
Substrate to filament distance	2 cm	2 cm

### 3.4 Characterization Technique

#### 3.4.1 Scanning electron microscope (SEM)

The SEM is perhaps the most routinely utilized instruments for the characterization of nano-materials. With an SEM it is possible to obtain secondary electron images of organic and inorganic materials within nanoscale resolution by allowing topographical and morphological studies to be carried out with the use of scanning electron beam across a surface and monitoring the secondary electrons emitted. Morphology study for the FESEM images of the nanowires in this study were obtained by using a Hitachi SU 8000 SEM at low electron accelerating voltage of 2 kV. A schematic diagram of this SEM is shown in Fig. 3.10.

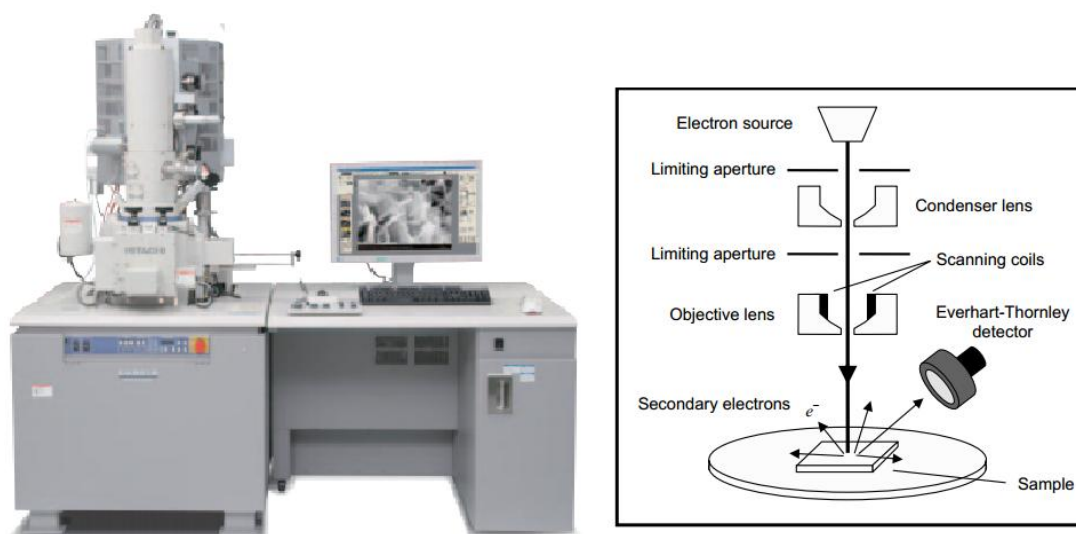


**Fig. 3.10** Hitachi SU 8000 SEM picture and schematic diagram of SEM ("Characterization Techniques for Nanomaterials," 2008).

#### 3.4.2 Energy dispersive X-ray (EDX)

Energy dispersive X-ray (EDX) spectroscopy uses an incident electron to eject an orbital electron and thus ionized the atom. Then, an electron from an outer electron

orbital will fill into the vacant shell immediately to resume the steady state. An excess energy is produced in this process during electron transition and an x-ray is emitted. Due to the reason where the difference in energy between two orbitals takes on a value unique to the element, the energy of the emitted x-ray is also unique to the element. Hence, this X-ray is called a “characteristic x-ray”, which is used for elemental analysis. Fig. 3.12 show Schematic diagram of EDX. The spectrum was collected by Hitachi SU 8000 at 15 kV. The working distances for the imaging and EDX were fixed at 8 mm and 15 mm respectively.

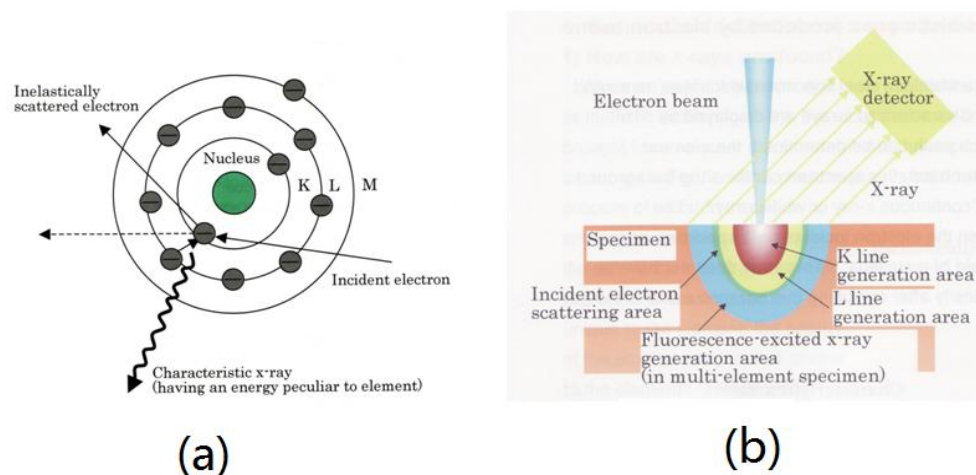


**Fig. 3.11** Schematic diagram of EDX basic principle. (a) Generation of characteristic X-ray in sodium (Na) atom model. (b) X-ray schematic diagram ("Characterization Techniques for Nanomaterials," 2008).

### 3.4.3 Transmission electron microscope (TEM)

In a TEM, a beam of focused high energy electrons is transmitted through a thin sample to reveal information about its morphology, crystallography, particle size distribution and its elemental composition. This technique is capable in providing atomic-resolution lattice images, as well as giving chemical information at a spatial resolution of 1 nm. Due to the reason where the unique physical and chemical properties

of nanomaterials are not only depend on their composition, but also on their structures, TEM can serve as a powerful tool for characterizing and understanding such structures. TEM is unique as it can be used to focus on a single nanoparticle in a sample, and directly identify and quantify its chemical and electronic structure. Perhaps the most important application of TEM is the atomic resolution real-space imaging of nanoparticles (Lin, Lu, Tu, & Ren, 2004). TEM and HRTEM images of the nanowires were obtained by means of a TEM (JEOL JEM-2100F) with an accelerating voltage of 200 kV. Elemental analysis and mappings for the nanowire were carried out by using STEM/HAADF and Oxford EDX detectors.

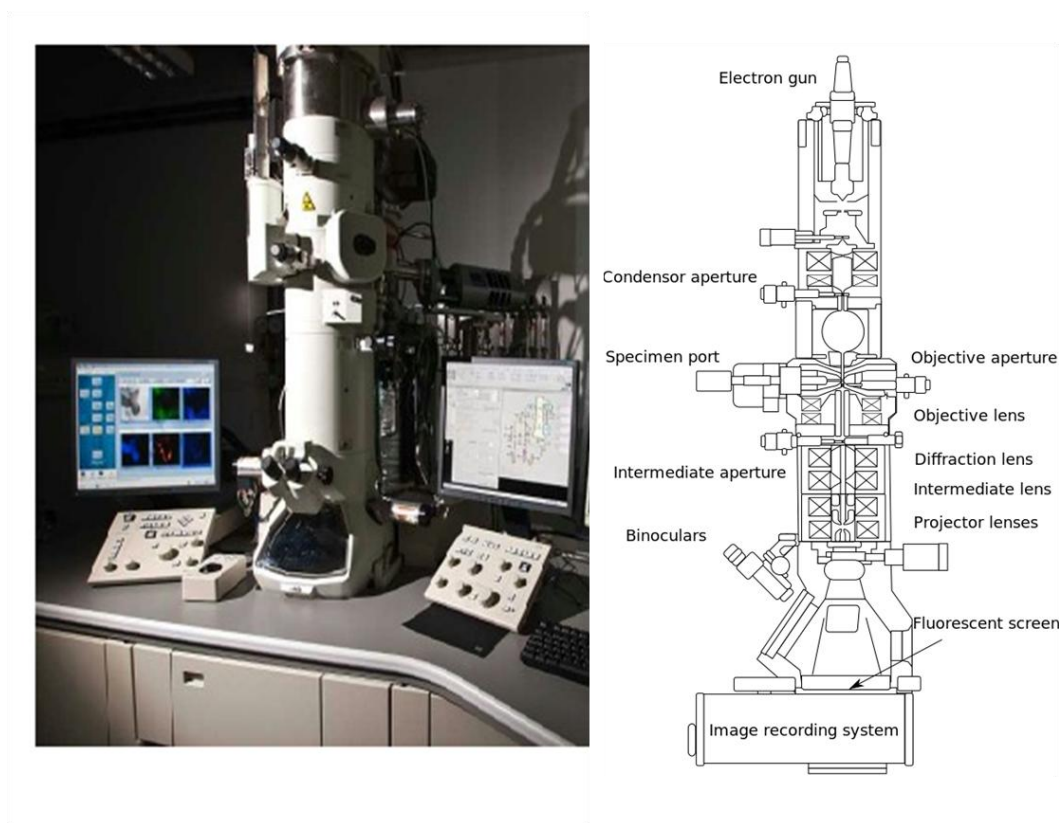


**Fig. 3.12** JEOL JEM-2100F TEM picture and schematic diagram of TEM ("Characterization Techniques for Nanomaterials," 2008).

#### 3.4.4 X-Ray diffraction (XRD)

XRD involves monitoring the diffraction of X-rays after they interact with the sample. It is a crystallographic technique used for identifying and quantifying various crystalline phases that present in solid materials and powders. In XRD, the crystal structure can be determined as well as the size of grains and nanoparticles. When X-rays are directed at a regular crystalline sample, a proportion of them are diffracted to produce a pattern. From such a pattern the crystal phases can be identified by comparison to those of internationally recognized databases (such as International Center of Diffraction Data ICDD) that contain reference patterns. In current study, crystalline characteristics the sample can analyzed by using a SIEMENS D5000 X-ray diffractometer in the  $2\theta$  range from  $20^\circ$  to  $80^\circ$  at a fixed grazing incidence angle of  $5^\circ$ . The step time and step size of the scanning were fixed to 3 seconds and  $0.02^\circ$ , respectively.

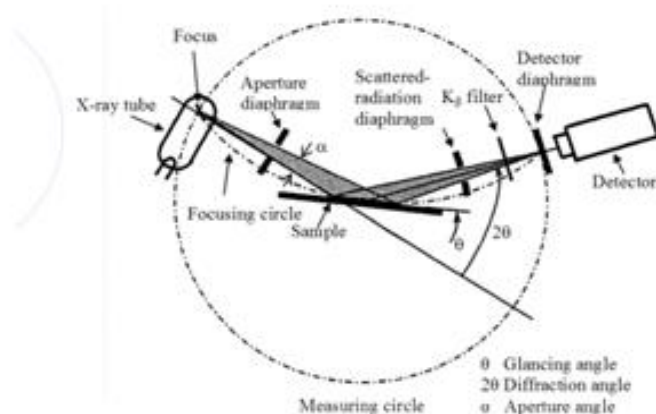
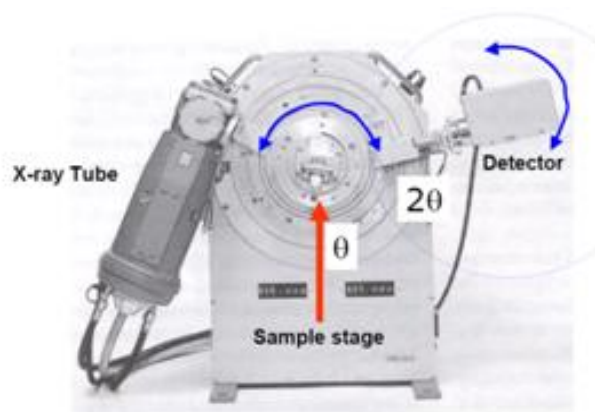


**Fig. 3.13** Schematic diagram of XRD ("Characterization Techniques for Nanomaterials," 2008).

### 3.4.5 Raman spectroscopy

Phase analysis for Raman spectra of the thin film samples were recorded by using an InVia Raman microscope (Fig. 3.15a) with a charge-coupled device detector and a grating of 2400 lines/mm. The argon ion laser with an excitation wavelength and laser power of 514 nm and 10 mW respectively, was used. Similarly, the optical properties of the sample were measured spectrometer. Raman spectroscopy is based on monitoring the intensity and wavelength of light that is scattered inelastically from molecules or crystals (Fig. 3.15b). It is suitable for characterizing organic and inorganic samples. In a Raman experiment, a sample is irradiated with light of known polarization and wavelength (generally in the visible or infrared ranges). Inelastic (or Raman) scattering

occurs and the scattered light is wavelength-shifted with respect to the incident light. The spectrum of the scattered light is then analyzed to determine the changes in its wavelength. Raman spectroscopy is a powerful analytical tool for qualitatively and quantitatively investigating the composition of materials.

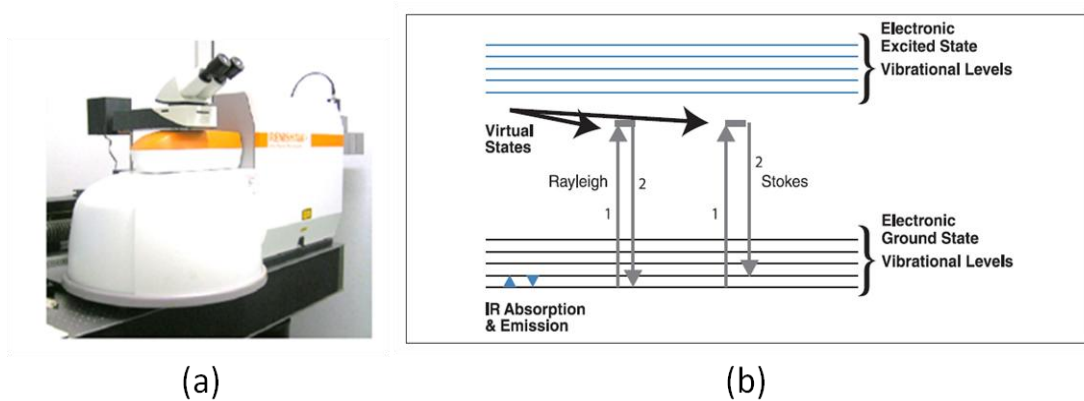


**Fig. 3.14** InVia Raman microscope picture and representation of Raman scattering ("Characterization Techniques for Nanomaterials," 2008).

#### 3.4.6 I-V measurement

A KEITHLEY Model 236 Source Measure Unit (Fig. 3.16a) instrument was used to measure the I-V characteristics of the nanowires. This instrument address a wide variety of applications, including the characterization of semiconductor devices and the measurement of leakage currents or insulation resistance. Samples use silver paste and electrode pins to connect with the source measure unit (SMU) (Fig. 3.16b). The range of I-V measurement from -4V to +4.5V (sweep rate is 0.1V).



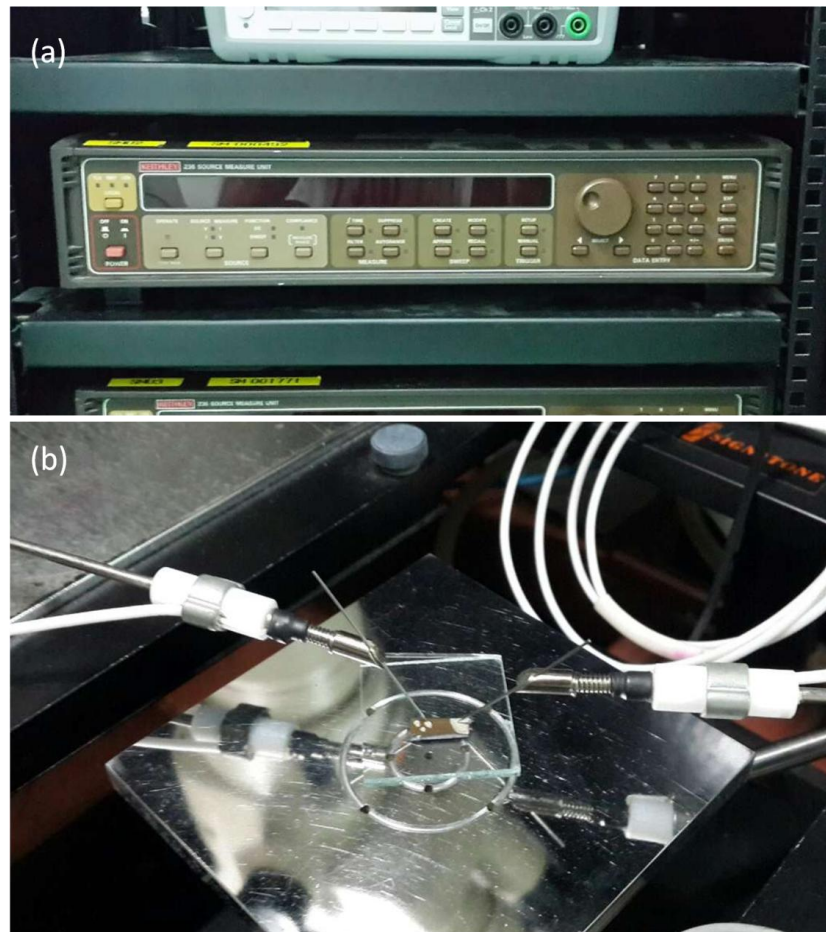


**Fig. 3.15** (a) KEITHLEY Model 236 source measure unit and (b) electrode pins.

The schematic diagram of the cross-sectional view for the fabricated Si-based nanowire heterojunction is shown in Fig.3.16. one of electrode connected to shell of nanowires. Another electrode connected to NiSi layer. And it also connected to the core of nanowires.

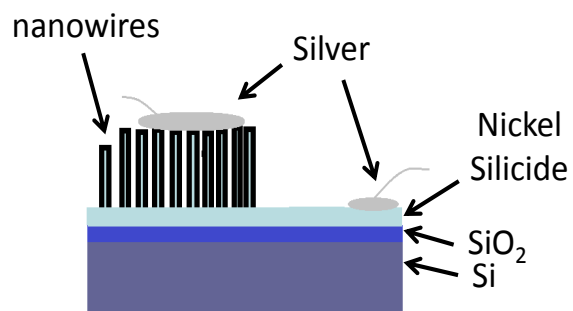


**Fig. 3.16** A schematic diagram of the fabricated Si-based nanowires heterojunction structure and the electrodes configuration.



## CHAPTER 4

### RESULTS AND DISCUSSIONS

#### 4.1 Effects of filament temperature on substrate surface temperature

Figure 4.1 shows the variations of substrate temperature and substrate surface on Si and glass substrates with filament temperature during the deposition. The substrate temperature,  $T_b$  is referred to the measured temperature on the bottom surface of the substrate while the surface temperatures are measured on surface of the substrate for c-Si ( $T_s$ ) and glass substrates ( $T_g$ ) respectively. As can see from the figure, the  $T_s$  and  $T_g$  show significant higher temperature compared to the  $T_b$ . According to literature, thermal irradiation from hot-filament easily inducing additional heat effects on the substrate surfaces. However, the decomposition of  $\text{SiH}_4$ ,  $\text{CH}_4$  and  $\text{H}_2$  in HWCVD processes involving radicals mainly of  $\text{SiH}_3$ ,  $\text{CH}_3$  and  $\text{H}$ . The  $\text{H}$  radicals have been reported to highly dependent on the heating effect on substrate surface. Therefore, the higher temperatures of the substrate surfaces are attributed to hydrogen assisted thermal effect.

The surface temperature demonstrated an obvious increment with increase of the filament temperature. The  $T_b$  showed a slight increase for the filament temperature at  $1950^\circ\text{C}$ . Increase in filament temperature enhances the decomposition rate of the radicals especially  $\text{H}$  radicals. Thus large flux of  $\text{H}$  radicals impinges on the substrate surfaces and consequently rising the surface temperature. Moreover, the  $T_g$  shows a slightly higher temperature compared to  $T_s$ . This is attributed to the lower heat dissipation in glass substrate as compared to the c-Si substrate.

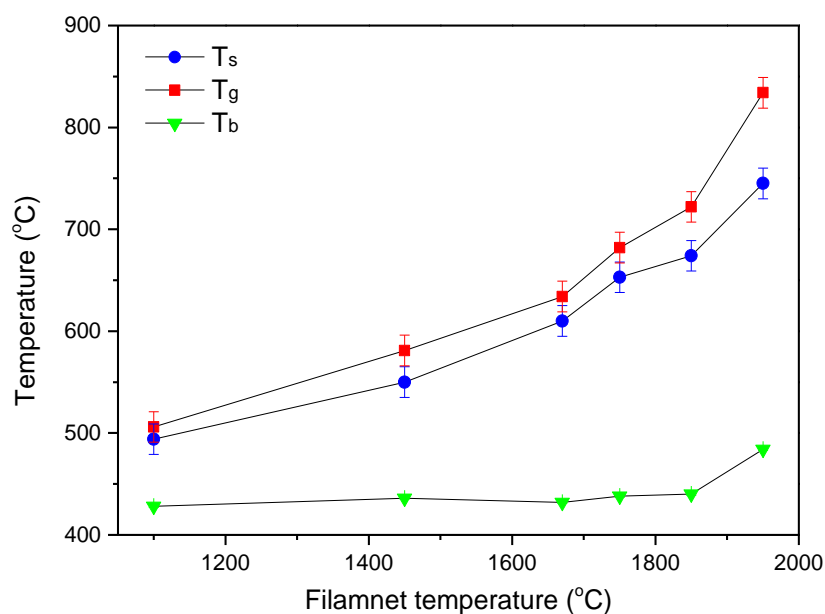


**Fig. 4.1** Variations of substrate temperature and substrate surface on Si and glass substrates with filament temperature.

## 4.2 Surface morphologies of nanowires

The surface morphologies of Si-based nanowires prepared by HWCVD at different filament temperatures on crystal Si substrates are demonstrated in Fig. 4.2. At 1150°C, short NiSi nanowires are found to grow uniformly and well-distributed on the SiO<sub>2</sub> surface. These short nanowires with the estimated average diameter of 20 nm were grown on top of conical-like solid particles (as shown in the inset). This would be the bud for the core nanowire in growing of core-shell nanowires at the high filament temperatures [Fig. 4.2(b) ~ (f)].

At low filament temperature of 1150°C, there is almost no decomposition of SiH<sub>4</sub>, CH<sub>4</sub> and H<sub>2</sub> by hot-filament. Therefore, the impinging of these molecules on the surface of Ni nanoparticles at substrate temperature of 450°C was catalytically decomposed by Ni nanoparticles. Diffusion of the Si-rich species into the Ni nanoparticles induces the growth of these buds of the NiSi nanowires.

The growth of these NiSi nanowires could follow the nucleation limited silicide

reaction which has been described by Kim et al. (J. Kim & Anderson, 2005). Increase in filament temperature to 1450°C, high density of rod-like Si nanowires is clearly presented in Fig. 4.2(b). These nanowires demonstrated a grainy surface morphology as demonstrated in the inset figure. The estimated average diameter and length of these nanowires are typically 400 nm and 2 µm respectively that measured in Fig. 4.2.

At filament temperatures 1450°C and above, the hot-filament is able to decompose the SiH<sub>4</sub> and H<sub>2</sub> efficiently (Tange et al., 2001). High decomposition rates of SiH<sub>4</sub> and H<sub>2</sub> lead to deposition of high density of Si-rich species onto the surface of Ni nanoparticles. This increases the diffusion of Si-rich species into the Ni nanoparticles thus enhances the precipitation of Si nanowires. On the other hand, deposition of the decomposed radicals mainly SiH<sub>3</sub> on the sidewalls of the nanowires leads to the radial growth of the Si grains as shown by the grainy morphology in the figure. This morphology is significant for the nanowires at 1650°C.

Further increase in filament temperature to 1750°C and above has resultant in drastical changes in the morphology of the nanowires. These nanowires demonstrated a smooth surface and irregular array. Furthermore, these nanowires exhibited longer and slimmer in length and diameter, respectively. At filament temperature of 1750°C, the estimated average diameter and length are 70 nm and 4 µm respectively. As presented by Dasgupta et al. (Tange et al., 2001), filament temperature above 1750°C demonstrated sufficiently decomposition of SiH<sub>4</sub>, H<sub>2</sub> and CH<sub>4</sub> molecules. In this case, additional diffusion of the C-rich species could easily limit the radial growth of Si nanocolumns which has been reported in our previous work (Chong, Dee, Yahya, & Rahman, 2013; Chong et al., 2011). The formation of SiC as a shell layer could easily

prevent the growth of the nanowires radially. Therefore, these nanowires show whisker-like nanowires with small in diameter as compared to the Si nanowires grown at 1450°C.

Furthermore, it is worth noticeably that the nanowires demonstrated branched nanoneedles at the stem of the nanowires that have been grown at 1850°C. The formation of these branched nanoneedles seems to be grown on the NiSi particles on the sidewalls of the nanowires. The formation of the NiSi nanoparticles could be due to the out-diffusion of NiSi from the core of nanowires. The out-diffusion of the metal catalysts during the growth of nanowires has been observed also by Hannon et al. (Hannon, Kodambaka, Ross, & Tromp, 2006). The estimated average tip radius of the sharp nanoneedles is about 5 nm. These hierarchical ultra-sharp nanoneedles on the sidewalls of the nanowires can provide an extremely strong local field effect in field emission application.

At last, when the filament temperature is adjusted to 1950°C the diameter of nanowires increase to 150 nm and the surface become more smooth.

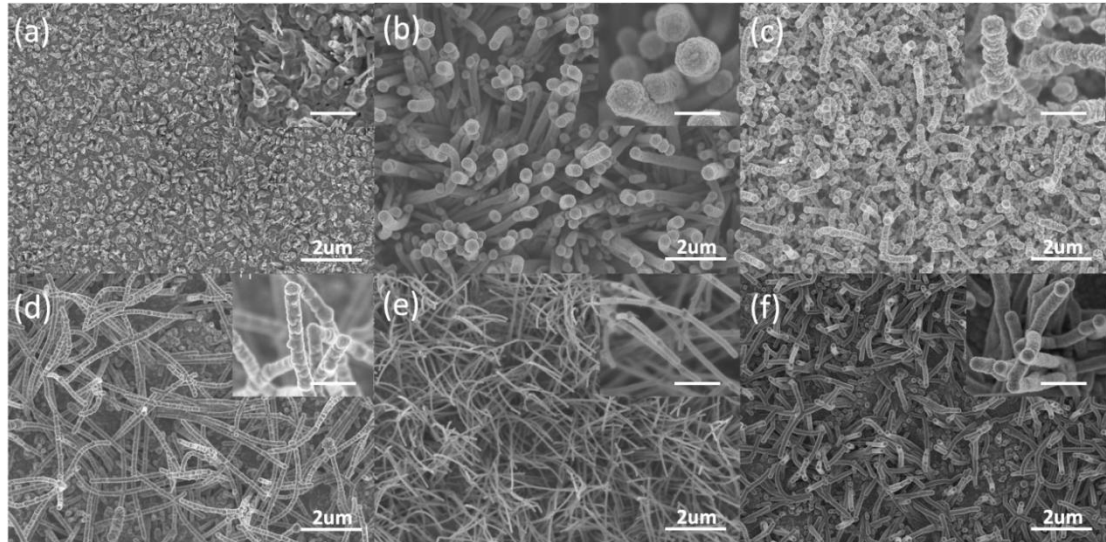


**Fig. 4.2** FESEM images of the Si-based nanowires synthesis by HWCVD on silicon at different filament temperatures (a) 1150°C, (b) 1450°C, (c) 1650°C, (d) 1750°C, (e) 1850°C, (f) 1950°C. Insets show the high magnification image of the nanowires. (Insets bar is 500 nm).

The nanowires grown on glass substrates at different filament temperatures are shown on Fig. 4.3. These nanowires exhibit a similar change with the nanowires grown on c-Si substrates in the variation with filament temperature. At low filament temperature of 1150°C, the nanowires demonstrated similar morphology as the nanowires grown on c-Si substrates. The thin nanowires grow into a larger diameter as rod-like nanowires at filament temperature of 1450~1650°C. At higher filament temperatures of 1750°C and above turns the nanowires into the NiSi/SiC core-shell heterostructures. Then crystal structure show the top of nanowire with filament temperature increase to 1950°C. Owing to the relatively high thermal resistance of glass substrate as compared to the c-Si substrate, the increase in surface temperature due to the hydrogen heat assisted transfer, on glass substrate is higher than c-Si substrate [Fig. 4.2]. As a result, the surface mobility of the growth increases and therefore enhances the surface diffusion of the growth species. This eventually leads to the film growth

conditions instead of growing nanowires.

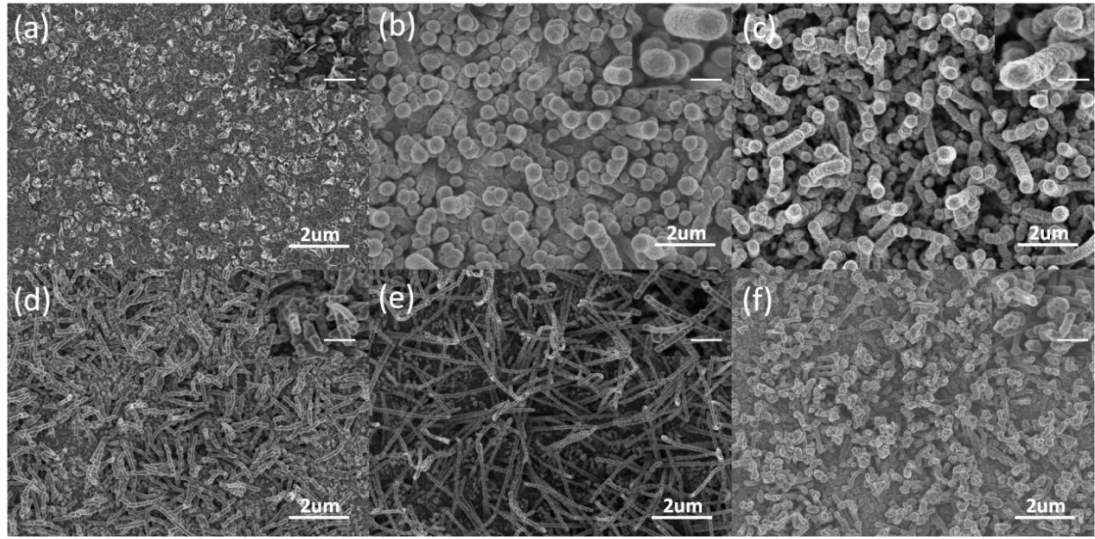


**Fig. 4.3** FESEM images of the nanowires synthesis by HWCVD on glass at different filament temperatures. (a) 1150°C, (b) 1450°C, (c) 1650°C, (d) 1750°C, (e) 1850°C, (f) 1950°C. Insets show the high magnification image of the nanowires. (Insets bar is 500 nm).

Fig. 4.4 show the variations of nanowire diameter on c-Si and glass with different filament temperature. The diameters of nanowire on c-Si substrate ( $D_s$ ) and on glass ( $D_g$ ) are measured by SEM result. At low filament temperature of 1150°C, small buds of the NiSi nanowires growth with diameter about 20 nm. Then the diameter of nanowire increase sharply to the top of the curve, formed nanowires with diameter more than 300 nm. It is observed that diameter of nanowire on glass is more big than it on c-Si..

At the filament temperature higher than 1450°C, the diameter decrease with filament temperature. The nanowire with the smallest is estimated diameter to be 70 nm when filament temperature of 1850°C. Therefore, the diameter increases again at filament temperature of 1950°C.

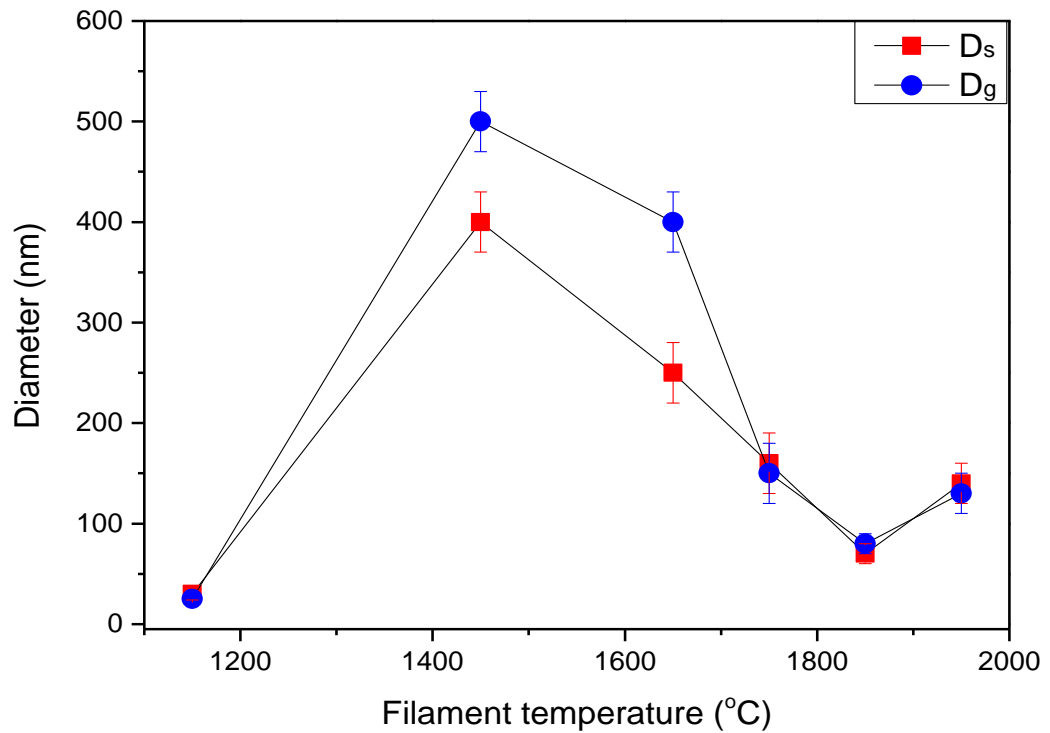


**Fig. 4.4** Variations of nanowire diameter with filament temperature on silicon and glass substrate.

### 4.3 Cross-sectional view study

The cross-section FESEM images of typical nanowires prepared at filament temperature above 1850°C are shown in Fig. 4.5. These images show more detailed information including the surface topography, compositions and internal structure of the nanowires. Fig. 4.5(a) shows secondary electron image that clearly presented the nanowires grown on top of NiSi/SiO<sub>2</sub>/c-Si. The use of SiO<sub>2</sub> is to prevent the diffusion of Ni into the c-Si substrate when the substrate was heated to a temperature above 350°C. The estimated thickness of the NiSi layer is about 140 nm. Increase in thickness of the deposited Ni layer is due to the diffusion of Si and C into the Ni nanoparticles thus forming NiSi layer. This NiSi subsequently catalyzed the growth of the Si and NiSi/SiC core-shell nanowires at filament temperatures of 1450 and 1850°C,

respectively.

As can see from the figure, the nanowires grown in vertically aligned however the alignment of the nanowires is not uniform when it's grown longer. Moreover, the surface of the nanowires is smooth and less granny as compared to the Si nanowires grown at 1450°C (inset of Fig. 4.2(b)). The backscattered electron image of the cross-section nanowires is illustrated in Fig. 4.5(b). The images showed presence of bright particles stick on the surface of the nanowires. Generally, the BSE (backscattered electron) image was used to illustrate the distribution of heavier elements that were presented on the surface of the nanostructures. The high density of metals gave a significant contrast compared to the matrix in the BSE image. Apparently bright particles on the surface of the nanowires reveal the presence of NiSi nanoparticles. These NiSi nanoparticles were found randomly distributed on surface along the nanowires. The formation of these NiSi nanoparticles could be due to the out-diffusion of NiSi from the core of the nanowires during the growth process. These NiSi nanoparticles are deduced to serve as a solid catalyst that inducing the growth of the hierarchical ultra-sharp nanoneedles on the sidewalls of the nanowires as mentioned above.

Fig. 4.5(c) demonstrates a backscattered electron signal of the nanowires that detected by external photo-diode backscattered electron (PDBSE) detector. By applying higher electron accelerating voltage of 15 kV, the internal structure of the nanowires can be clearly observed through the image as shown in the inset figure. Furthermore, the compositions distribution also can be significantly illustrated by the PDBSE image. The PDBSE image clearly revealed heterostructure core-shell nanowires, where the core and



shell are attributed to NiSi and SiC respectively. Moreover, the NiSi core can be clearly presented along the nanowires from the root to the tip. The formation of the NiSi nanoparticles also clearly presented on the surface along the nanowires. On the other hand, these nanowires are grown on top of NiSi layer and the core nanowires are tightly connected to the NiSi layer, which could be a good electrical contact for energy storage applications such as lithium-ion batteries and micro-supercapacitor electrodes. An extremely large surface area of the nanowires is expected to enhance the performance of these devices.

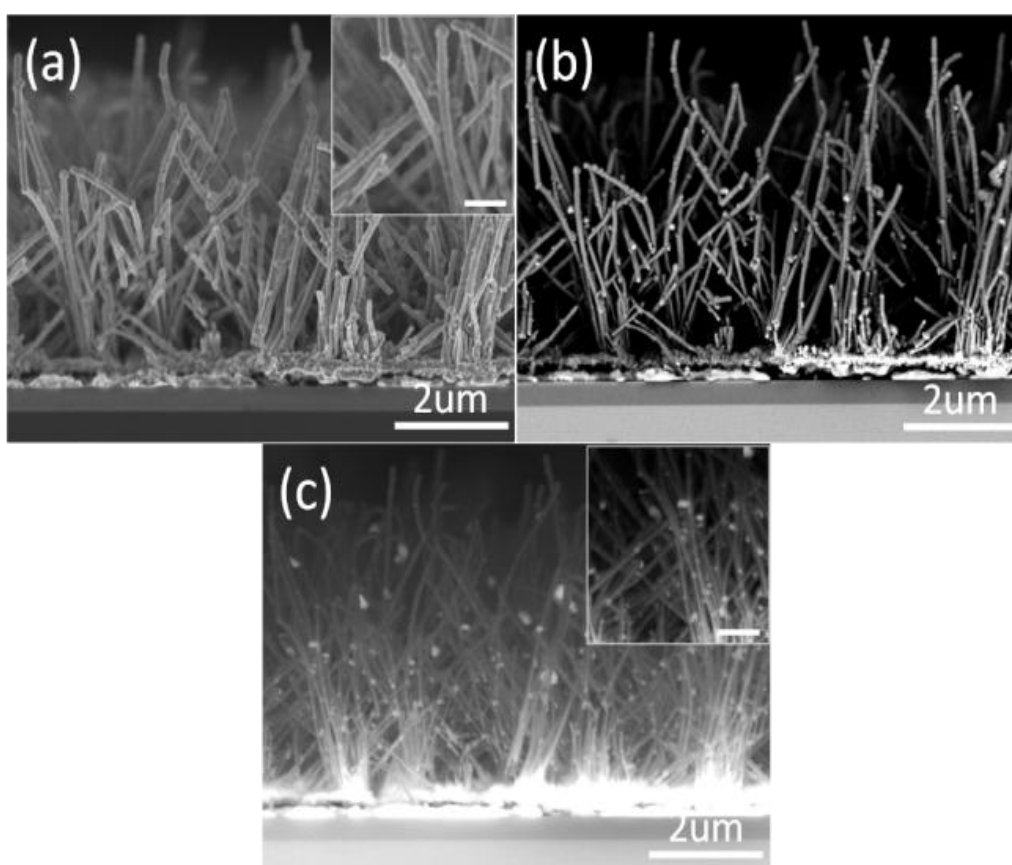


**Fig. 4.5** Cross-sectional view of FESEM images of the nanowires prepared by HWCVD at filament temperature of 1850°C. (a) secondary electron (b) backscattered electron signals (c) backscattered electron signal collected by a photo-diode backscattered electron (PDBSE) detector that attached to the SEM. Insets figures present high magnification of the FESEM images.

#### 4.4 Microstructure study

The microstructures of the nanowires were investigated by HRTEM and the result for the samples that have been grown at filament temperatures of 1450 and 1850°C are shown in Fig. 4.6 and Fig. 4.7, respectively. These nanowires were prepared on top of a carbon film that has been supported by a TEM copper-grid as demonstrated in the TEM images.

According to Fig. 4.6, the nanowire exhibits a flower-like morphology with a core-shell structure. The formation of the flower branches implies that the radial growth has taken place which transform into nanocolumns and ultimately led to the branching topology. The diameter and thickness of the core and shell are estimated to be 10 and 130 nm, respectively. There is no obvious tapered morphology observed on the nanowire, which indicates that the shell was grown along the axis of the nanowires that are parallel with the core.

Fig. 4.6(b) shows a HRTEM image that was obtained at the sidewall of nanowire, which reveals a polycrystalline structure of the nanocolumns. The estimated spacing was estimated to be approximately 0.31 nm, which corresponds to Si (111) crystallographic plane [JCPDS card no: 78-2500]. The crystal orientation is further revealed by the Fast Fourier Transform (FFT) as shown in the inset image.

The polycrystalline Si that formed nanocolumns can be observed in Fig. 4.6(d). The estimated diameter of these nanocolumns is approximately to be in the range between 20 and 24 nm. The formation of these nanocolumns follows the preferred orientation of Si (111) crystalline plane and also the growth direction as well. Furthermore, a thin amorphous layer can be clearly observed on the outer layer of the

nanowire, which indicates the indicating a formation of thin amorphous  $\text{SiO}_x$  that could be attributed to an oxidation on the nanowire surface after exposed to ambient. The estimated thickness of the amorphous  $\text{SiO}_x$  layer was approximately 3.4 nm.

Fig. 4.6(c) depicts a HRTEM image along the edge of the core for a nanowire, which clearly reveals a single crystalline core and a polycrystalline shell heterostructure. The lattice spacing is approximately estimated to be 0.33 nm and well, correspond to a crystallographic plane of  $\text{Ni}_3\text{Si}_2$  (112) orientation [JCPDS card no: 89-7167]. This indicates that the core of the nanowires was actually formed by a single crystalline  $\text{Ni}_3\text{Si}_2$  nanowire. The single crystalline  $\text{Ni}_3\text{Si}_2$  structure of the core of nanowire was further revealed by an FFT as shown in the inset. Furthermore, the FFT result reveals the growth of these  $\text{Ni}_3\text{Si}_2$  core nanowires are oriented along the (112) crystal plane.



crystallographic plane of NiSi (121) orientation [JCPDS card no: 70-2626]. The single crystalline NiSi structure of the core of nanowire was further revealed by an FFT image as shown in the inset. Furthermore, the FFT result reveals the growth of these Ni<sub>3</sub>Si<sub>2</sub> core nanowires are oriented along the (021) crystal plane.

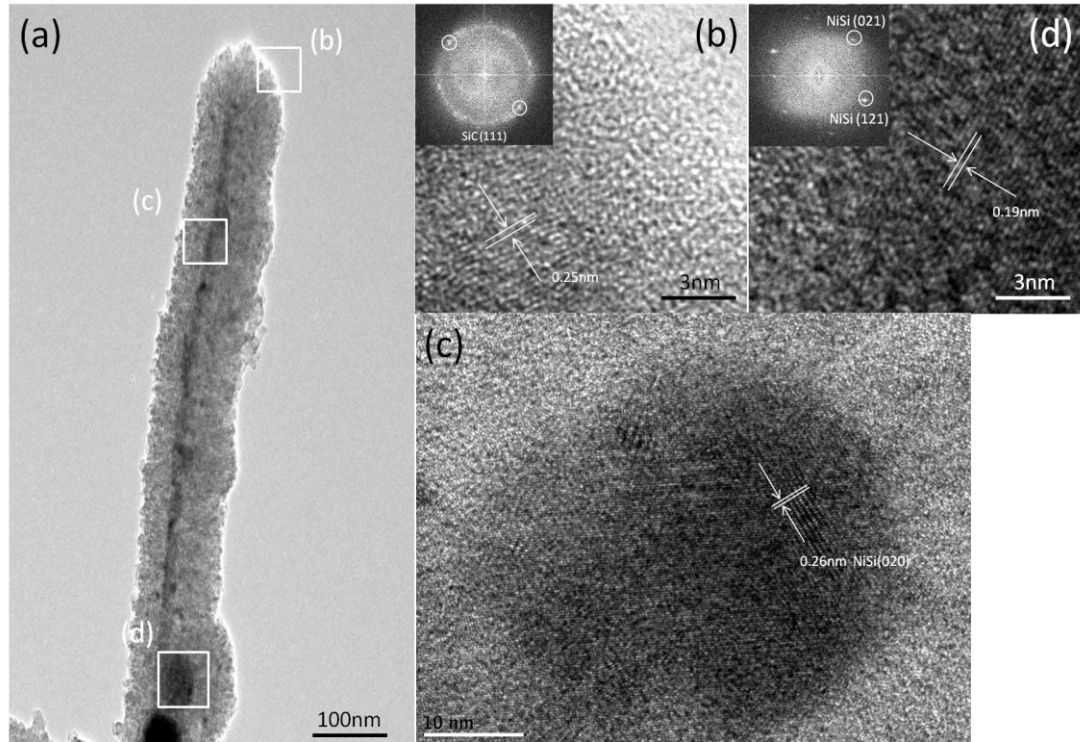


**Fig. 4.7** (a) TEM morphology of the NiSi/SiC core-shell NWs prepared at filament temperature 1850°C. (b) and (d) HRTEM image of the NWs enlarged from the frame in (a) show a insert particle inside the NW.

#### 4.5 Compositions studies of a single nanowire by EDS elemental mappings

The compositions of a single nanowire were investigated by using STEM/EDS mappings with a HAADF detector, as illustrated in Fig. 4.8. Fig. 4.8(a) shows a dark-field STEM image of a single nanowire with a clear core-shell structure. This image area was used for the EDS elemental mappings. The compositions of the nanowire are demonstrated by the EDS maps as shown in Figs. 4.8(b) to (e) that

correspond to the C, Ni, Si and O respectively.

From these maps, the core-shell nanowire is mainly consisted of C, Ni and Si. Little O was appeared in the O map indicates that the formation of thin layer of amorphous SiO<sub>x</sub> that is due to the oxidation effect on the nanowire surface. The Ni was clearly revealed in the Ni map that implies the NiSi core nanowire. Appearance of uniformly distribution of the Si and C along the length of the nanowire in their respective maps supports the formation of SiC shell nanowire. It is worth notice that the Ni and Si maps reveal the compositions of the NiSi nanoparticles formation at the root of the nanowire due to the NiSi out-diffusion. This can be clearly presented in the bright-field image, and the elemental maps of Ni and Si.

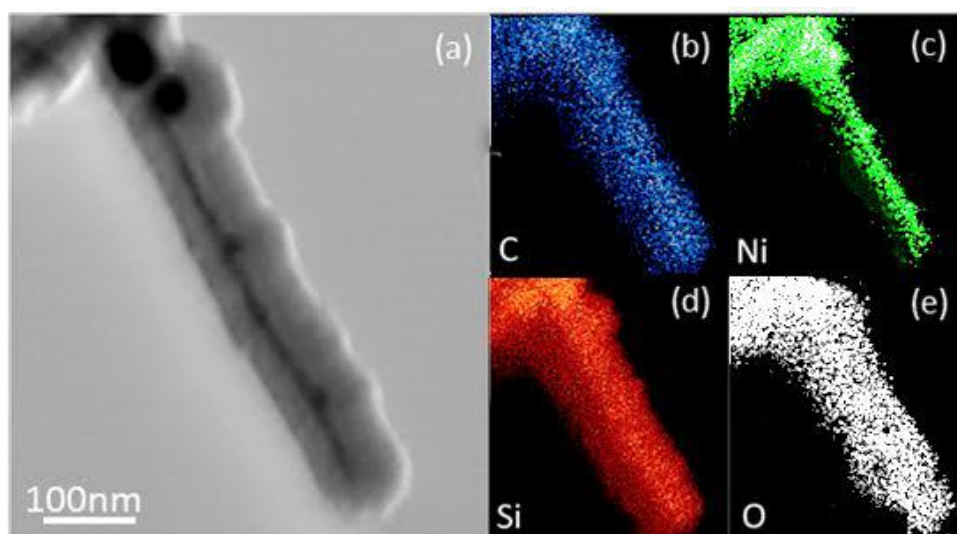


**Fig. 4.8** (a) Bright-field TEM image of a single nanowire, (b) ~ (e) EDS element maps of the core-shell nanowire.

#### 4.6 Phases and orientation studies

Fig. 4.9 shows the XRD patterns of the nanowires prepared on c-Si substrates at different filament temperatures. The samples demonstrated mainly the presence of three major phases of crystalline nickel silicide which include NiSi, Ni<sub>2</sub>Si and Ni<sub>3</sub>Si<sub>2</sub> in the

sample. Crystalline NiSi with the orientation of (211) plane seems to be dominant among the phases. This indicates that the NiSi core could be in (211) growth direction. Instead of NiSi, other phases of NiSi could be from the NiSi nanoparticles that presence on the surface along the nanowires. Since the formation of the NiSi nanoparticles is random therefore its cause to the formation of different crystalline planes.

Furthermore, crystalline Si peaks were observed at diffraction angles of 28.4 and 56.3° which are correspond to crystalline Si (111) and (311) planes respectively. At highest filament temperature of 1850°C, a small and broad peak was detected at diffraction angle of 35.7° which attributed to crystalline 3C-SiC with a crystalline orientation of (111) plane. The crystalline size of the SiC nano-crystallites can be estimated by using Scherrer's equation as  $D = k\lambda / (\beta \cos\theta)$ , where  $k$ ,  $\lambda$ ,  $\beta$  and  $\theta$  are corresponding to the Scherrer's constant (0.9), wavelength of X-ray (1.5089 Å), full-width half-maximum of the diffraction peak and Bragg angle of the diffraction peak respectively (Goh, Wah, Aspanut, & Rahman, 2014). The average crystallite size of the SiC nano-crystallites is about 3 nm. By rough estimation from the PDBSE image, the diameter of the core and shell is about 7 and 70 nm respectively. Therefore, the presence SiC nano-crystallites most probably embedded within an amorphous matrix in the shell of the nanowires.

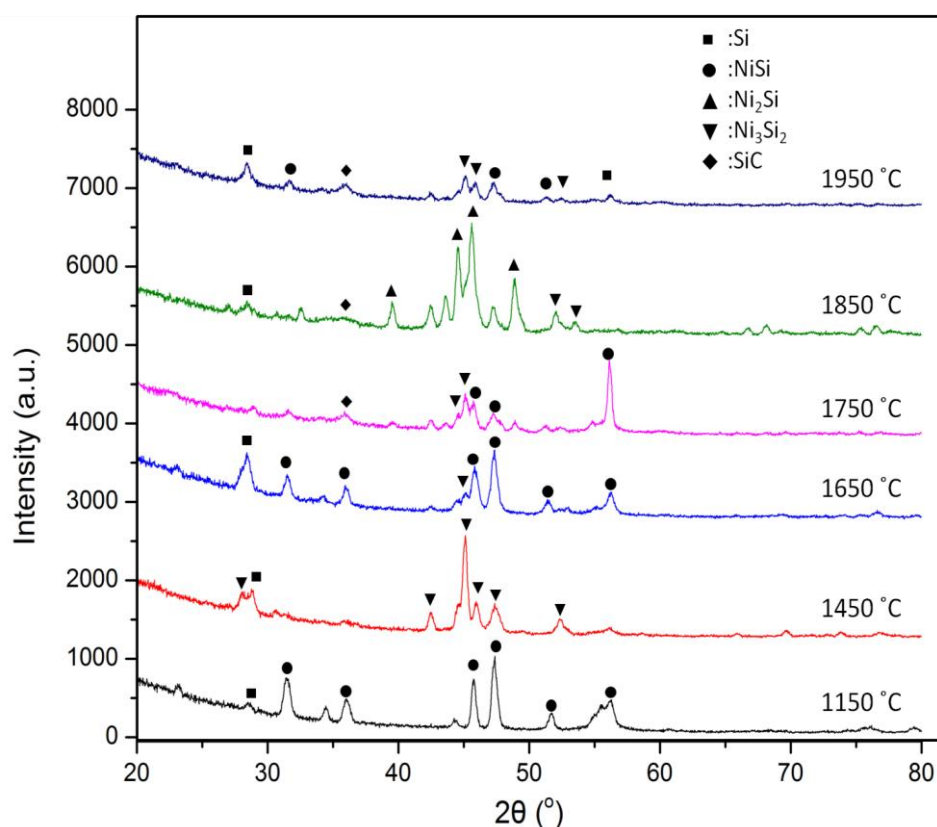


**Fig. 4.9** XRD spectra of the nanowires prepared by HWCVD at different filament temperatures.

The percentage of phases presented in the samples prepared at different filament temperatures are determined by obtaining their areas using Gaussian fitting method ( Fig. 4.10 ). At lowest filament temperature of 1150°C, the sample mainly consisted on NiSi phase with a little amount of crystalline Si phase. At this filament temperature, there is no decomposition of  $\text{SiH}_4$  and  $\text{CH}_4$  by hot-filament. Diffusion of the  $\text{SiH}_4$  molecules on the Ni nanoparticles was decomposed by the Ni nanoparticles catalytically. However, the catalytically decomposition usually happened at a very low decomposition rate of  $\text{SiH}_4$ . Therefore, only small amount of crystalline Si phase has been observed and the formation of the NiSi phase is most dominant through the diffusion of Si into the Ni nanoparticles.

With increased of the filament temperature to 1450°C, most of the NiSi phase



are converted to  $\text{Ni}_3\text{Si}_2$  and the percentage of crystalline Si phase increases. This could be the reason for the growth of Si nanowires which catalyzed mainly by  $\text{Ni}_3\text{Si}_2$  phase. Then at high filament temperature of  $1650^\circ\text{C}$ , the percentage of NiSi and Si phases increase cause of  $\text{SiH}_4$  decomposed rate increase. Further increase in filament temperature up to  $1750^\circ\text{C}$  allows the SiC and  $\text{Ni}_2\text{Si}$  phases to be appeared. At this filament temperature, the filament was capable to decompose the  $\text{CH}_4$  molecules and the decomposition rate of  $\text{CH}_4$  increases with further increase in filament temperature above  $1750^\circ\text{C}$ . Then filament temperature increase to  $1850^\circ\text{C}$ , the  $\text{Ni}_3\text{Si}_2$  phase decreased with increase of  $\text{Ni}_2\text{Si}$  and SiC phases. The conversion of  $\text{Ni}_3\text{Si}_2$  to  $\text{Ni}_2\text{Si}$  may be due an increase of surface temperature which is attributed to the hydrogen assisted heat transfer from the hot-filament at temperature of  $1850^\circ\text{C}$ .

Furthermore, high decomposition rate of  $\text{CH}_4$  leads to the diffusion of the C-rich species into the NiSi nanoparticles subsequently forms SiC layer radially. Formation of these  $\text{Ni}_2\text{Si}$  and SiC phases eventually precipitated as  $\text{Ni}_2\text{Si}$  core and SiC shell of the heterostructures nanowires. Increase in surface temperature increases the solubility of C into the NiSi nanoparticles thus relatively reduces the amount of Si in the NiSi phase (50 % of Si in NiSi at  $1150^\circ\text{C}$ , 40 % of Si in  $\text{Ni}_3\text{Si}_2$  at  $1450^\circ\text{C}$ , and 33 % of Si in  $\text{Ni}_2\text{Si}$  at  $1850^\circ\text{C}$ ). This would eventually results to the thin and long whisker-like nanowires due to the formation of the SiC shell layer which limited the radial growth of Si nanocolumns. At highest filament temperature of  $1950^\circ\text{C}$ , the  $\text{Ni}_2\text{Si}$  phase disappeared with increase of other phases (Si, SiC,  $\text{Ni}_2\text{Si}$  and NiSi). High surface temperature due to the hydrogen assisted heat transfer effect had lead to the fully conversion of  $\text{Ni}_2\text{Si}$  to other Si related phases.

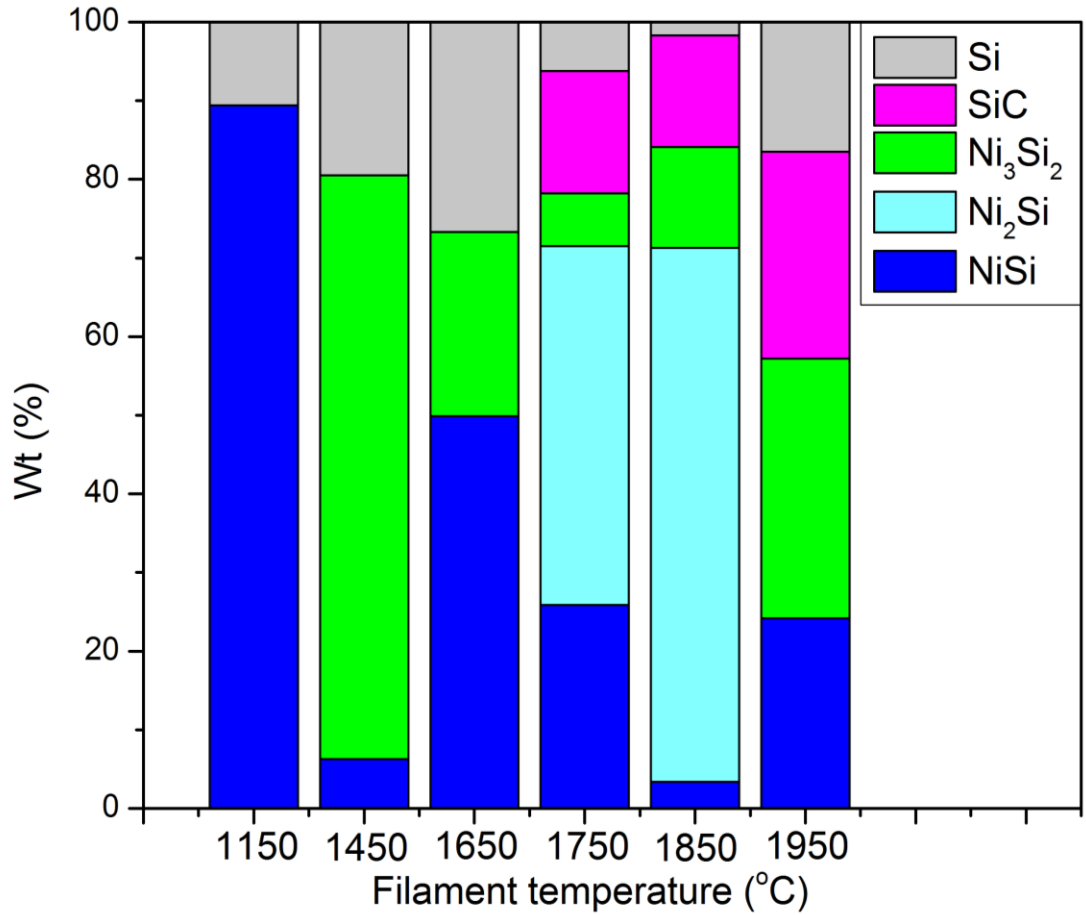


**Fig. 4.10** Weight percentage of phases presented in the samples prepared by HWCVD at different filament temperatures.

#### 4.7 Structural properties study

The Raman scattering spectra of the nanowires prepared on different substrates and at different filament temperatures are shown in Fig. 4.11. These Raman spectra are mainly consist of NiSi, Si and SiC excitation bands. Fig. 4.11(a) and (b) show Raman excitation bands of NiSi at filament temperature of 1150°C for the samples that had been prepared on c-Si and glass substrates. The excitation bands of NiSi phases are located at 196, 213, 295 and 367  $\text{cm}^{-1}$ . A small Raman excitation band appeared at 520  $\text{cm}^{-1}$  corresponds to transverse optical (TO) of crystalline Si which is attributed to the Raman excitation band of c-Si substrate. With increasing the filament temperature up to

1450°C and 1650°C, a sharp crystalline Si (TO) excitation band near to 520  $\text{cm}^{-1}$  is clearly shown in the Raman spectra for both substrates. The full spectra of the crystalline Si (TO) excitation band are shown in the insets of Figs. 4.11(c) and (d). Obviously, the appearance of these crystalline Si (TO) bands is attributed to the Si nanowires instead of c-Si substrate since the crystalline Si (TO) band also shown for the samples prepared on glass substrate. Furthermore, other Si phases are also clearly observed at 150, 300 and 960  $\text{cm}^{-1}$  which are correspond to the transverse acoustic (TA), longitudinal acoustic (LA), longitudinal optical (LO), and second order of TO (2TO) for amorphous Si vibrational modes respectively (Tong, Muhamad, & Rahman, 2012). The excitation band at around 620  $\text{cm}^{-1}$  could probably relate to Si-H vibration mode of hydrogenated amorphous Si. The dominant phase of crystalline Si component with small amount of its amorphous component implies the crystalline Si core and amorphous Si shell of these heterostructures core-shell nanowires. The growth of these heterostructures NiSi/Si core-shell nanowires have been reported previously. At highest filament temperatures between 1750 and 1950°C, all the Si excitation bands almost disappeared with presence of SiC bands at 780 and 910  $\text{cm}^{-1}$  that correspond to TO and LO of SiC vibrational modes respectively. This reveals formation of 3C-SiC nano-crystallites embedded within an amorphous matrix. Owing to the heterostructures of NiSi/SiC core-shell nanowires, thus these SiC nano-crystallites probably embedded within an amorphous SiC shell. The appearance of D and G bands at 1300  $\text{cm}^{-1}$  and 1600  $\text{cm}^{-1}$  respectively, for the samples at 1650 [Fig. 4.11(c)] and 1850°C [Fig. 4.11(f)] indicates a formation of C components on the nanowires which could be due to the sufficient decomposition of  $\text{CH}_4$  in the gas-phase reactions at hot-filament temperature

above 1600°C.

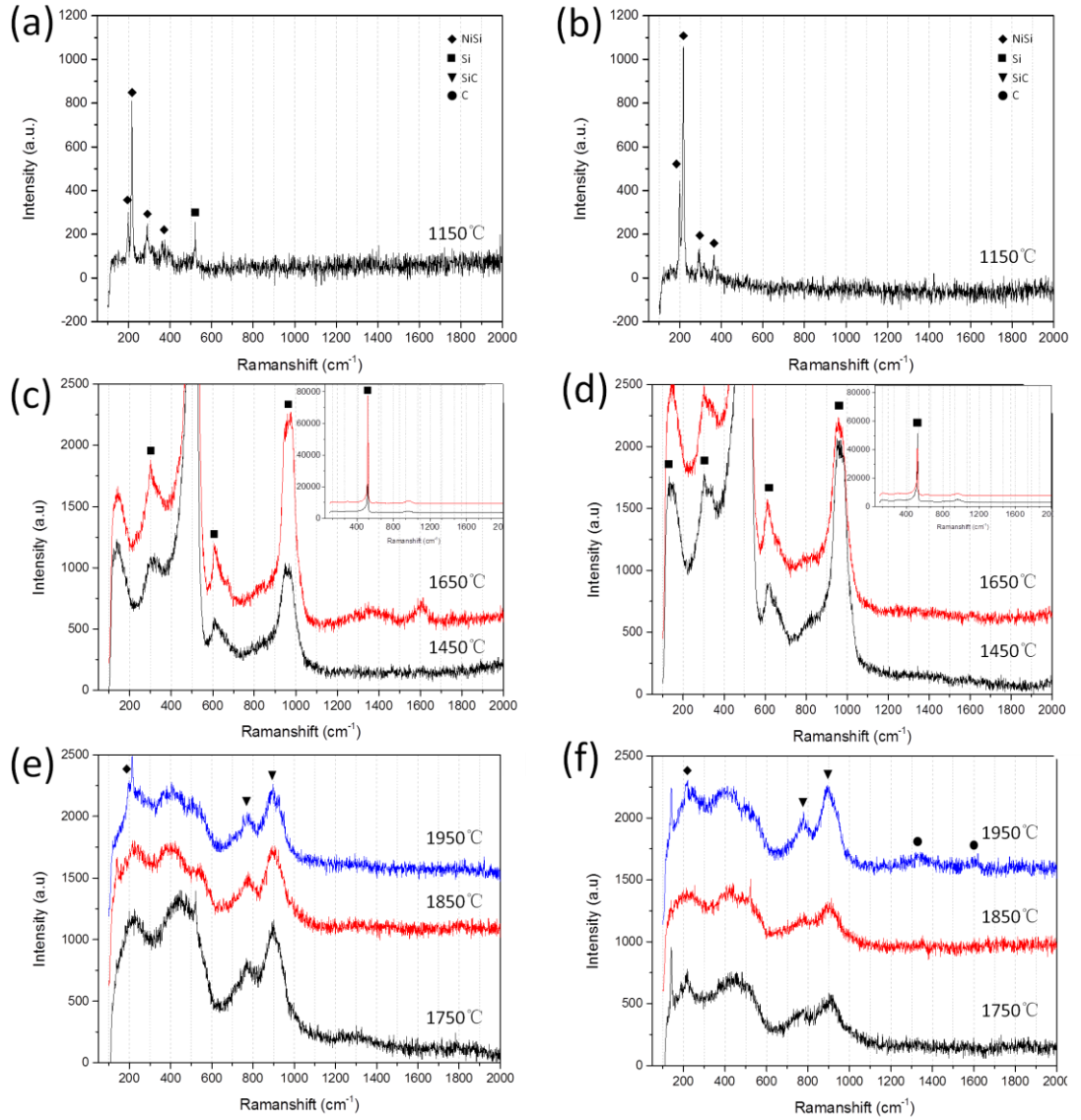


**Fig. 4.11** Raman scattering spectra of the nanowires prepared by HWCVD at different filament temperatures. (a), (c) and (e) is filament temperature 1150°C ~ 1950°C on silicon substrates. (b), (d) and (f) is filament temperature 1150°C ~ 1950°C on glass substrates.

#### 4.8 Optical properties study by photoluminescence emission spectra

The optical properties of the nanowires were studied by using photoluminescence emission. Fig. 4.12 shows the PL spectra at different nanowires grown on the silicon filament temperature by HWCVD. The photoluminescence spectrum has been measured by the excitation source He-Cd laser. Photons have been

detected wavelength range 400 to 900 nm, which covers the entire visible region PL emitted broad spectrum. The PL spectra of Gaussian decomposition components are shown in Fig. 4.12. These decomposed PL emission spectra consist of 5 components located 450, 525, 600, 690 and 760 nm.

There are two strong emission bands centred at around 600 and 690 nm and three small emission bands at around 450, 525 and 760 nm. The emission bands in the range of 650-800 nm is reported to be originated from the quantum confinement effect of the Si nano-crystallites embedded with an amorphous matrix (Ali, 2007; XY Chen et al., 2005; Iacona, Franzò, & Spinella, 2000). The emission band in the range of 550-650 nm is generally referred to the emission due to the oxygen related defects and/or to surface and interface effects (Dinh, Chase, Balooch, Siekhaus, & Wooten, 1996; Iacona et al., 2000; Inokuma et al., 1998). Si nanocrystallites create an intermediate state in the formation of NC-Si/SiO<sub>2</sub> interface, the electron-hole radiative recombination, resulting in emission in the visible region strongly. Has been described according to the quantum confinement effect by Trwoga model (Trwoga, Kenyon, & Pitt, 1998). There are silicon nanocrystals that diameter less than 10 nm matrix embedded in amorphous shell, so it leads a widened band gap than bulk crystal Si (1.12 eV at room temperature), and at T<sub>f</sub> 1850°C appear two small peaks in visible range at 450 and 525 nm indicate fluorescent silicon carbide nanostructures emissions (Liang et al., 2000; D.-H. Wang et al., 2008; Xi et al., 2005). The peak at 450 nm is comparable to the PL emissions from SiC nanowires (Liang et al., 2000; D.-H. Wang et al., 2008) or crystalline SiC nanoparticles (Xi et al., 2005). As a summary, the various PL emissions from the nanowires have revealed that the PL emissions strongly depend on the quantum confinement effects

attributed to size of the nano-crystallites embedded in the nanowires.

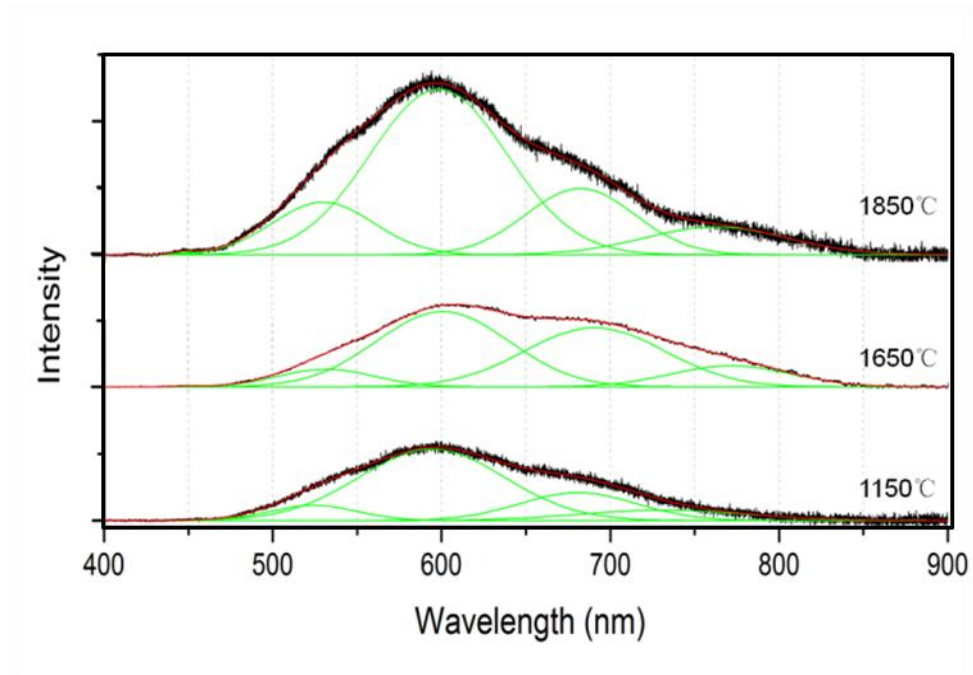
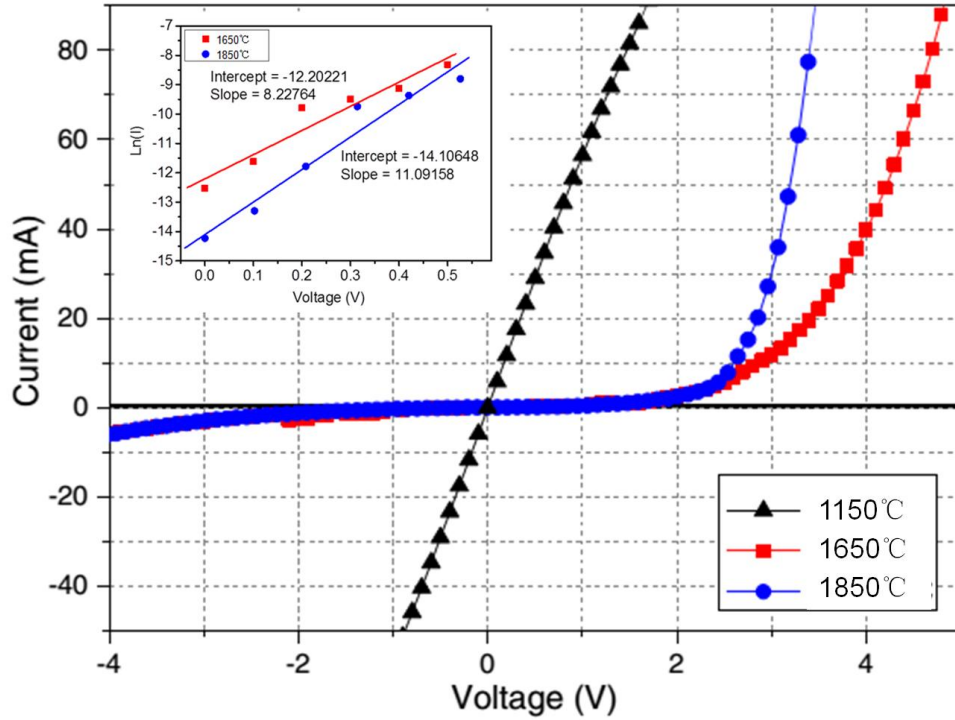


**Fig. 4.12** Photoluminescence (PL) spectra for the nanowires on silicon substrate at different filament temperatures.

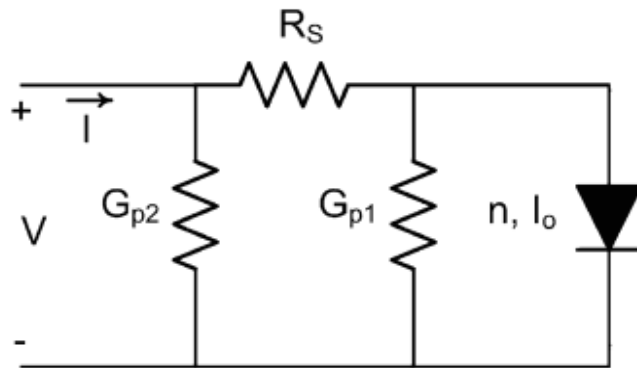
#### 4.9 Electrical properties study

Fig. 4.13 shows the I-V measurement of the different types of Si-based heterostructures nanowires. The schematic diagram of the cross-sectional view for the fabricated Si-based nanowires heterojunction is shown in Fig. 3.16. For the I-V measurement, the structure was contacted with silver paste and the effective area of about  $0.785 \text{ mm}^2$ . I-V curves of the Si-based nanowires at different filament temperatures are demonstrated in Fig. 4.13. At filament temperature of  $1150^\circ\text{C}$ , NiSi nanowires showed a linear I-V curve indicates a significant resistance model. At filament temperature  $1450$  and  $1850^\circ\text{C}$  the Si-based heterostructures core-shell nanowires show a clear diode characteristic in I-V curves. Inset of the figure of Fig.

4.13 presents the logarithmic current against voltage ( $\ln I$ - $V$ ) plot of the NiSi/Si and NiSi/SiC core-shell nanowires prepared at filament temperatures of 1450 and 1850°C.



**Fig. 4.13** I-V curves of the samples prepared by HWCVD at different filament temperatures. Inset of the figure presents the logarithmic current against voltage ( $\ln I$ - $V$ ) plot of the NiSi/Si and NiSi/SiC core-shell nanowires prepared at filament temperatures of 1450 and 1850°C



**Fig. 4.14** Generic diode model with parasitic series resistance and parallel conductances.

I consider a universal ideal diode junction diode emulation by single exponential, parasitic series resistance ( $R_s$ ) is modeled, and the sake of completeness, and include

the loss mechanisms of the two branches: the parasitic parallel conductance,  $G_{P1}$  and  $G_{P2}$  of junction and surrounding areas. Fig. 4.14 Equivalent circuit model presented here.

The equation of I–V characteristics mathematical model of this circuit is given (Ortiz-Conde & Sánchez, 2005):

$$I = I_o \left\{ \exp \left[ \frac{q(V - IR_s)}{nkT} \right] - 1 \right\} + (V - IR_s)G_P + VG_{P2}(1 + R_s G_{P1}) \quad (6)$$

where  $n$  is the ideality factor,  $I_o$  is reverse saturation current,  $T$  is the temperature in Kelvin,  $q$  the electronic charge and  $k$  is the Boltzmann constant.  $G_p$  and  $R_s$  are the parallel parasitic conductances and series resistance respectively, which are important parameters that influence the electrical characteristics of diodes.

It is well known that using a common basic function, the above equation can not be clearly distinguished beyond general  $I$  or  $V$ . Therefore, it has become accustomed to the use of explicit approximate solution for modeling purposes. Several of these approximate solutions have been proposed, which uses only the basic functions. But now, as  $I$  and  $V$  clear precise analytical solutions already exist (Ortiz-Conde & Sánchez, 2005), used to be known Lambert  $W$  function, a special role, which does not express a special function in the elementary analysis functionality.

For this heterojunction diode the influence of  $G_{P2}$  can be ignored and written function like this:

$$I = I_o \left\{ \exp \left[ \frac{q(V - IR_s)}{nkT} \right] - 1 \right\} + (V - IR_s)G_P \quad (7)$$

At very small voltage region, the  $n$  was obtained from slope of the  $\ln I$ - $V$  plot Fig.



4.13(b),

$$n = \frac{q}{kT} \left( \frac{\partial V}{\partial \ln I} \right) \quad (8)$$

Compare to the ordinary diode, the Si-based heterojunction diodes showed a relatively larger ideality factor. The larger ideality factor could be due to a combination of metal-semiconductor junctions and other heterojunctions in series, and each node has a corresponding ideality factor. The ideality factor of Si-based heterojunction diode equal to the superposition of all as described below (Shah, Li, Gessmann, & Schubert, 2003):

$$n = \sum_i n_i \quad (9)$$

The equation (7) has four unknown parameters which are  $n$ ,  $I_0$ ,  $R_s$  and  $G_p$ . by Using (I, V) experimental data that can solve this equation. Since there are 4 unknowns and more than four (I, V) or simultaneous equations that cannot expect to get values for  $n$ ,  $I_0$ ,  $R_s$  and  $G_p$  that would exactly satisfy all equations. For this reason I used the least square fitting approach which gives us the opportunity of using more data points and hence increasing the accuracy of the solution. The values of  $n$ ,  $I_0$ ,  $R_s$  and  $G_p$  obtained by this method are also given in Table 3.

TABLE 3: The experimental values of the parameters obtained from I–V fittings.

Type of diode	Ideality factor	Reverse saturation current (A/cm <sup>2</sup> )	Series resistance (Ω)	Parallel conductances (1/Ω)
NiSi/Si	4.701	1.583E-4	6.132	0
NiSi/SiC	3.487	6.125E-8	4.772	8.306E-4

## CHAPTER 5

### CONCLUSION

The growth, structural and electrical properties of the Ni-catalyzed Si-based nanowires prepared by HWCVD at different filament temperatures has been investigated. Different types of Si-based heterostructures nanowires have been successfully grown by HWCVD at different filament temperatures. The structural and electrical properties of the nanowires are presented.

The filament temperature played an important role in controlling the decomposition mechanism, in which of the source gases and gas phase reactions thus led to the growth of different types of the Si-based heterostructures nanowires. The growth of NiSi nanowires at low filament temperature followed the solid phase diffusion of the Si into Ni nanoparticles where the  $\text{SiH}_4$  was catalytically decomposed by the Ni nanoparticles. Increase in the filament temperature involved the decomposition of the source gases by hot-filament and promotes growth of the NiSi/Si and NiSi/SiC heterostructures core-shell nanowires at 1450 and 1850°C, respectively. Formation of thin and long NiSi/SiC core-shell nanowires was attributed to the diffusion of C-rich species formed SiC shell layer radially which limited the radial growth of Si nanocolumns. Both NiSi/Si and NiSi/SiC heterostructures core-shell nanowires exhibited heterojunction electrical characteristic which could be used for nanoscale diode applications. Those properties prove that silicon based heterostructures nanowires can be used for versatile sensor at harsh environment. Future work is in progress to understand the correlation between work function and conductance results,

and how to assemble the nanowire device effectively is also need be studied.

## REFERENCES

- Ali, Atif Mossad. (2007). Origin of photoluminescence in nanocrystalline Si: H films. *Journal of luminescence*, 126(2), 614-622.
- Bae, Joonho, Kim, Hyunjin, Zhang, Xiao-Mei, Dang, Cuong H, Zhang, Yue, Choi, Young Jin, . . . Wang, Zhong Lin. (2010). Si nanowire metal–insulator–semiconductor photodetectors as efficient light harvesters. *Nanotechnology*, 21(9), 095502.
- Bandaru, PR, & Pichanusakorn, P. (2010). An outline of the synthesis and properties of silicon nanowires. *Semiconductor science and technology*, 25(2), 024003.
- Bhatnagar, Mohit, & Baliga, B Jayant. (1993). Comparison of 6H-SiC, 3C-SiC, and Si for power devices. *Electron Devices, IEEE Transactions on*, 40(3), 645-655.
- Bi, Jinghui, Wei, Guodong, Wang, Lin, Gao, Fengmei, Zheng, Jinju, Tang, Bin, & Yang, Weiyou. (2013). Highly sensitive piezoresistance behaviors of n-type 3C-SiC nanowires. *J. Mater. Chem. C*, 1(30), 4514-4517.
- Borowiak-Palen, E, Ruemmeli, MH, Gemming, T, Knupfer, M, Biedermann, K, Leonhardt, A, . . . Kalenczuk, RJ. (2005). Bulk synthesis of carbon-filled silicon carbide nanotubes with a narrow diameter distribution. *Journal of applied physics*, 97(5), 056102.
- Casady, JB, & Johnson, R Wayne. (1996). Status of silicon carbide (SiC) as a wide-bandgap semiconductor for high-temperature applications: A review. *Solid-State Electronics*, 39(10), 1409-1422.
- Characterization Techniques for Nanomaterials. (2008) *Nanotechnology-Enabled Sensors*: Springer US.
- Chen, Xihong, Xing, Yingjie, Xu, Jun, Xiang, Jie, & Yu, Dapeng. (2003). Rational growth of highly oriented amorphous silicon nanowire films. *Chemical physics letters*, 374(5), 626-630.
- Chen, XY, Lu, YF, Tang, LJ, Wu, YH, Cho, BJ, Xu, XJ, . . . Song, WD. (2005). Annealing and oxidation of silicon oxide films prepared by plasma-enhanced chemical vapor deposition. *Journal of Applied Physics*, 97(1), 014913.

- Choi, Nam-Soon, Yao, Yan, Cui, Yi, & Cho, Jaephil. (2011). One dimensional Si/Sn-based nanowires and nanotubes for lithium-ion energy storage materials. *Journal of Materials Chemistry*, 21(27), 9825-9840.
- Chong, Su Kong, Dee, Chang Fu, Yahya, Noorhana, & Rahman, Saadah Abdul. (2013). Control growth of silicon nanocolumns' epitaxy on silicon nanowires. *Journal of nanoparticle research*, 15(4), 1-8.
- Chong, Su Kong, Goh, Boon Tong, Aspanut, Zarina, Muhamad, Muhamad Rasat, Dee, Chang Fu, & Rahman, Saadah Abdul. (2011). Radial growth of slanting-columnar nanocrystalline Si on Si nanowires. *Chemical Physics Letters*, 515(1), 68-71.
- Cohen-Karni, Tzahi, Casanova, Didier, Cahoon, James F, Qing, Quan, Bell, David C, & Lieber, Charles M. (2012). Synthetically encoded ultrashort-channel nanowire transistors for fast, pointlike cellular signal detection. *Nano letters*, 12(5), 2639-2644.
- Colgan, EG, Gambino, JP, & Cunningham, B. (1996). Nickel silicide thermal stability on polycrystalline and single crystalline silicon. *Materials chemistry and physics*, 46(2), 209-214.
- Cui, Yi, Lauhon, Lincoln J, Gudiksen, Mark S, Wang, Jianfang, & Lieber, Charles M. (2001). Diameter-controlled synthesis of single-crystal silicon nanowires. *Applied Physics Letters*, 78(15), 2214-2216.
- Curley, Ronald, McCormack, Thomas, & Phipps, Matthew. Low-pressure CVD and Plasma-Enhanced CVD.
- Dai, Hongjie, Wong, Eric W, Lu, Yuan Z, Fan, Shoushan, & Lieber, Charles M. (1995). Synthesis and characterization of carbide nanorods. *Nature*, 375(6534), 769-772.
- Das, Sachindra Nath, Myoung, Jae-Min, & Kar, Jyoti Prakash. (2011). *Junction properties and applications of ZnO single nanowire based Schottky diode*: INTECH Open Access Publisher.
- Dinh, LN, Chase, LL, Balooch, M, Siekhaus, WJ, & Wooten, F. (1996). Optical properties of passivated Si nanocrystals and SiO<sub>x</sub> nanostructures. *Physical Review B*, 54(7), 5029.
- Doyle, J, Robertson, R, Lin, GH, He, MZ, & Gallagher, A. (1988). Production of high-quality amorphous silicon films by evaporative silane surface decomposition. *Journal of Applied Physics*, 64(6), 3215-3223.

- Edwards, PL, & Happel Jr, RJ. (1962). Beryllium oxide whiskers and platelets. *Journal of Applied Physics*, 33(3), 943-948.
- Fan, Hong Jin, Werner, Peter, & Zacharias, Margit. (2006). Semiconductor nanowires: from self-organization to patterned growth. *small*, 2(6), 700-717.
- Fan, JY, Wu, XL, & Chu, Paul K. (2006). Low-dimensional SiC nanostructures: fabrication, luminescence, and electrical properties. *Progress in Materials Science*, 51(8), 983-1031.
- Feng, SQ, Yu, DP, Zhang, HZ, Bai, ZG, & Ding, Y. (2000). The growth mechanism of silicon nanowires and their quantum confinement effect. *Journal of Crystal Growth*, 209(2), 513-517.
- Feng, ZC, Mascarenhas, AJ, Choyke, WJ, & Powell, JA. (1988). Raman scattering studies of chemical-vapor-deposited cubic SiC films of (100) Si. *Journal of applied physics*, 64(6), 3176-3186.
- Fissel, A, Schr öter, B, & Richter, W. (1995). Low-temperature growth of SiC thin films on Si and 6H-SiC by solid-source molecular beam epitaxy. *Applied physics letters*, 66(23), 3182-3184.
- Fu, LJ, Liu, Hao, Li, C, Wu, YP, Rahm, E, Holze, R, & Wu, HQ. (2006). Surface modifications of electrode materials for lithium ion batteries. *Solid State Sciences*, 8(2), 113-128.
- Goh, Boon Tong, Wah, Chan Kee, Aspanut, Zarina, & Rahman, Saadah Abdul. (2014). Structural and optical properties of nc-Si: H thin films deposited by layer-by-layer technique. *Journal of Materials Science: Materials in Electronics*, 25(1), 286-296.
- Goh, Boon Tong, Muhamad, Muhamad Rasat, & Rahman, Saadah Abdul. (2012). Photoluminescence and structural properties of silicon nanostructures grown by layer-by-layer deposition. *Optical Materials*, 34(8), 1282-1288.
- Han, Nannan, Liu, Hongsheng, & Zhao, Jijun. (2015). Novel Magnetic Monolayers of Transition Metal Silicide. *Journal of Superconductivity and Novel Magnetism*, 28(6), 1755-1758.
- Hannon, JB, Kodambaka, S, Ross, FM, & Tromp, RM. (2006). The influence of the surface migration of gold on the growth of silicon nanowires. *Nature*, 440(7080), 69-71.
- Hao, Jian-Ying, Wang, Ying-Yong, Tong, Xi-Li, Jin, Guo-Qiang, & Guo, Xiang-Yun. (2012). Photocatalytic hydrogen production over modified SiC nanowires under

visible light irradiation. *international journal of hydrogen energy*, 37(20), 15038-15044.

- Hayden, Oliver, Agarwal, Ritesh, & Lieber, Charles M. (2006). Nanoscale avalanche photodiodes for highly sensitive and spatially resolved photon detection. *Nature materials*, 5(5), 352-356.
- He, Zhiqing, Wang, Lin, Gao, Fengmei, Wei, Guodong, Zheng, Jinju, Cheng, Xiaomin, . . . Yang, Weiyou. (2013). Synthesis of n-type SiC nanowires with tailored doping levels. *CrystEngComm*, 15(13), 2354-2358.
- Hibino, H, Tanabe, S, Mizuno, S, & Kageshima, H. (2012). Growth and electronic transport properties of epitaxial graphene on SiC. *Journal of Physics D: Applied Physics*, 45(15), 154008.
- Honda, Shin-ichi, Baek, Yang-Gyu, Ikuno, Takashi, Kohara, Hidekazu, Katayama, Mitsuhiro, Oura, Kenjiro, & Hirao, Takashi. (2003). SiC nanofibers grown by high power microwave plasma chemical vapor deposition. *Applied surface science*, 212, 378-382.
- Huang, Yu, Duan, Xiangfeng, Cui, Yi, & Lieber, Charles M. (2002). Gallium nitride nanowire nanodevices. *Nano Letters*, 2(2), 101-104.
- Iacona, Fabio, Franzò, Giorgia, & Spinella, Corrado. (2000). Correlation between luminescence and structural properties of Si nanocrystals. *Journal of Applied Physics*, 87(3), 1295-1303.
- Inokuma, T, Wakayama, Y, Muramoto, T, Aoki, R, Kurata, Y, & Hasegawa, S. (1998). Optical properties of Si clusters and Si nanocrystallites in high-temperature annealed SiO<sub>x</sub> films. *Journal of applied physics*, 83(4), 2228-2234.
- Jafari, A, Akbarnejad, E, Ghoranneviss, M, Yazdi, N Fasihi, & Rezaei, A. (2015). Effect of hot filament chemical vapour deposition growth method on tungsten carbide nanostructures. *Journal of Chemical Research*, 39(6), 328-331.
- Jing-Biao, CUI, Yu-Rong, MA, & Rong-Chuan, FANG. (1996). Effect of Filament Temperature on *in Situ* Absorption Spectrum and Diamond Film Growth. *CHINESE JOURNAL OF HIGH PRESSURE PHYSICS*, 10(2), 151-156. doi: 10.11858/gywlxb.1996.02.012
- Kalantar-zadeh, Kourosh, & Fry, Benjamin. (2007). *Nanotechnology-enabled sensors*: Springer Science & Business Media.
- Kern, Werner. (1970). Cleaning solutions based on hydrogen peroxide for use in silicon semiconductor technology. *RCA review*, 31, 187-206.

- Kim, C-J, Kang, Kibum, Woo, Yun Sung, Ryu, K-G, Moon, Heesung, Kim, J-M, . . . Jo, M-H. (2007). Spontaneous chemical vapor growth of NiSi nanowires and their metallic properties. *Advanced Materials*, 19(21), 3637-3642.
- Kim, Gi Bum, Yoo, Do-Joon, Baik, Hong Koo, Myoung, Jae-Min, Lee, Sung Man, Oh, Sang Ho, & Park, Chan Gyung. (2003). Improved thermal stability of Ni silicide on Si (100) through reactive deposition of Ni. *Journal of Vacuum Science & Technology B*, 21(1), 319-322.
- Kim, Joondong. (2010). *Nickel Silicide Nanowire Growth and Applications*: INTECH Open Access Publisher.
- Kim, Joondong, & Anderson, Wayne A. (2005). Spontaneous nickel monosilicide nanowire formation by metal induced growth. *Thin Solid Films*, 483(1), 60-65.
- Kolasinski, Kurt W. (2006). Catalytic growth of nanowires: vapor–liquid–solid, vapor–solid–solid, solution–liquid–solid and solid–liquid–solid growth. *Current Opinion in Solid State and Materials Science*, 10(3), 182-191.
- Komura, Yusuke, Tabata, Akimori, Narita, Tomoki, Kanaya, Masaki, Kondo, Akihiro, & Mizutani, Teruyoshi. (2007). Film Properties of Nanocrystalline 3C–SiC Thin Films Deposited on Glass Substrates by Hot-Wire Chemical Vapor Deposition Using CH<sub>4</sub> as a Carbon Source. *Japanese journal of applied physics*, 46(1R), 45.
- Komura, Yusuke, Tabata, Akimori, Narita, Tomoki, & Kondo, Akihiro. (2008). Influence of gas pressure on low-temperature preparation and film properties of nanocrystalline 3C-SiC thin films by HW-CVD using SiH<sub>4</sub>/CH<sub>4</sub>/H<sub>2</sub> system. *Thin Solid Films*, 516(5), 633-636.
- Lauhon, Lincoln J, Gudiksen, Mark S, Wang, Deli, & Lieber, Charles M. (2002). Epitaxial core–shell and core–multishell nanowire heterostructures. *Nature*, 420(6911), 57-61.
- Lavoie, C, d’Heurle, FM, Detavernier, Christophe, & Cabral, C. (2003). Towards implementation of a nickel silicide process for CMOS technologies. *Microelectronic Engineering*, 70(2), 144-157.
- Lee, Jeong Chul, Kang, Ki Hwan, Kim, Seok Ki, Yoon, Kyung Hoon, Song, Jinsoo, & Park, I Jun. (2002). Structural and electrical properties of polycrystalline silicon films deposited by hot-wire CVD. *Solar energy materials and solar cells*, 74(1), 233-245.
- Lee, Ki-Hong, Yang, Hyuck Soo, Baik, Kwang Hyeon, Bang, Jungsik, Vanfleet, Richard R, & Sigmund, Wolfgang. (2004). Direct growth of amorphous silica



- nanowires by solid state transformation of SiO<sub>2</sub> films. *Chemical physics letters*, 383(3), 380-384.
- Lee, Ki-Bum, Park, Sungho, & Mirkin, Chad A. (2004). Multicomponent magnetic nanorods for biomolecular separations. *Angewandte Chemie*, 116(23), 3110-3112.
- Li, Xiaodong, & Bhushan, Bharat. (1999). Micro/nanomechanical characterization of ceramic films for microdevices. *Thin Solid Films*, 340(1), 210-217.
- Li, YB, Xie, SS, Zou, XP, Tang, DS, Liu, ZQ, Zhou, WY, & Wang, G. (2001). Large-scale synthesis of  $\beta$ -SiC nanorods in the arc-discharge. *Journal of crystal growth*, 223(1), 125-128.
- Li, ZJ, Li, HJ, Chen, XL, Meng, AL, Li, KZ, Xu, YP, & Dai, L. (2003). Large-scale synthesis of crystalline  $\beta$ -SiC nanowires. *Applied Physics A*, 76(4), 637-640.
- Liang, CH, Meng, GW, Zhang, LD, Wu, YC, & Cui, Z. (2000). Large-scale synthesis of  $\beta$ -SiC nanowires by using mesoporous silica embedded with Fe nanoparticles. *Chemical Physics Letters*, 329(3), 323-328.
- Lin, Yuehe, Lu, Fang, Tu, Yi, & Ren, Zhifeng. (2004). Glucose biosensors based on carbon nanotube nanoelectrode ensembles. *Nano letters*, 4(2), 191-195.
- Liu, Chang, Li, Feng, Ma, Lai-Peng, & Cheng, Hui-Ming. (2010). Advanced materials for energy storage. *Advanced Materials*, 22(8), E28-E62.
- Lu, Qingyi, Hu, Junqing, Tang, Kaibin, Qian, Yitai, Zhou, Guien, Liu, Xianming, & Zhu, Jingsheng. (1999). Growth of SiC nanorods at low temperature. *Applied physics letters*, 75(4), 507-509.
- Mahan, AH, Carapella, J, Nelson, BP, Crandall, RS, & Balberg, I. (1991). Deposition of device quality, low H content amorphous silicon. *Journal of applied physics*, 69(9), 6728-6730.
- Marshall, Robert C. (1974). *Silicon carbide--1973: proceedings*: Univ of South Carolina Pr.
- Matsumura, Hideki. (1986). Catalytic Chemical Vapor Deposition (CTC-CVD) Method Producing High Quality Hydrogenated Amorphous Silicon. *Japanese journal of applied physics*, 25(12A), L949.
- Matsumura, Hideki, & Tachibana, Hiroyuki. (1985). Amorphous silicon produced by a new thermal chemical vapor deposition method using intermediate species SiF<sub>2</sub>. *Applied physics letters*, 47(8), 833-835.

- Matthews, JW, & Blakeslee, AE. (1974). Defects in epitaxial multilayers: I. Misfit dislocations. *Journal of Crystal Growth*, 27, 118-125.
- McAlpine, Michael C, Ahmad, Habib, Wang, Dunwei, & Heath, James R. (2007). Highly ordered nanowire arrays on plastic substrates for ultrasensitive flexible chemical sensors. *Nature materials*, 6(5), 379-384.
- Mehregany, M, Zorman, CA, Roy, S, Fleischman, AJ, & Rajan, N. (2000). Silicon carbide for microelectromechanical systems. *International materials reviews*, 45(3), 85-108.
- Mieszawska, Aneta J, Jalilian, Romaneh, Sumanasekera, Gamini U, & Zamborini, Francis P. (2007). The Synthesis and Fabrication of One-Dimensional Nanoscale Heterojunctions. *Small*, 3(5), 722-756.
- Morales, Alfredo M, & Lieber, Charles M. (1998). A laser ablation method for the synthesis of crystalline semiconductor nanowires. *Science*, 279(5348), 208-211.
- Ortiz-Conde, Adelmo, & Sánchez, Francisco J Garc ía. (2005). Extraction of non-ideal junction model parameters from the explicit analytic solutions of its I–V characteristics. *Solid-state electronics*, 49(3), 465-472.
- Pallecchi, E, Lafont, F, Cavaliere, V, Schopfer, F, Mailly, D, Poirier, W, & Ouerghi, A. (2014). High electron mobility in epitaxial graphene on 4H-SiC (0001) via post-growth annealing under hydrogen. *Scientific reports*, 4.
- Penn, Sharron G, He, Lin, & Natan, Michael J. (2003). Nanoparticles for bioanalysis. *Current opinion in chemical biology*, 7(5), 609-615.
- QI, Xue-Gui, CHANG, Chao, CHEN, Ze-Shao, WANG, Guan-Zhong, & LIAO, Yuan. (2003). Simulation and Analysis of Gas Phase Environment in HFCVD Diamond Films Growth. *Journal of Inorganic Materials*, 1, 031.
- Rao, CNR, Deepak, F Leonard, Gundiah, Gautam, & Govindaraj, Achutharao. (2003). Inorganic nanowires. *Progress in Solid State Chemistry*, 31(1), 5-147.
- Robertson, R, Hils, D, & Gallagher, A. (1984). Silane pyrolysis. *Chemical physics letters*, 103(5), 397-404.
- Robertson, Robert, & Gallagher, Alan. (1986). Reaction mechanism and kinetics of silane pyrolysis on a hydrogenated amorphous silicon surface. *The Journal of chemical physics*, 85(6), 3623-3630.
- Rurali, Riccardo. (2010). Colloquium: Structural, electronic, and transport properties of silicon nanowires. *Reviews of Modern Physics*, 82(1), 427.

- Salem, Aliasger K, Searson, Peter C, & Leong, Kam W. (2003). Multifunctional nanorods for gene delivery. *Nature materials*, 2(10), 668-671.
- Sarro, Pasqualina M. (2000). Silicon carbide as a new MEMS technology. *Sensors and Actuators A: Physical*, 82(1), 210-218.
- Schmidt, V, Wittemann, JV, & Gosele, U. (2010). Growth, thermodynamics, and electrical properties of silicon nanowires†. *Chemical reviews*, 110(1), 361-388.
- Schmidt, V., Wittemann, J. V., & Gösele, U. (2010). Growth, Thermodynamics, and Electrical Properties of Silicon Nanowires. *Chemical Reviews*, 110(1), 361-388. doi: 10.1021/cr900141g
- Shah, Jay M, Li, Y-L, Gessmann, Th, & Schubert, EF. (2003). Experimental analysis and theoretical model for anomalously high ideality factors ( $n \gg 2.0$ ) in AlGaIn/GaN pn junction diodes. *Journal of applied physics*, 94(4), 2627-2630.
- Suzuki, Hiroshi, Araki, Hiroshi, Tosa, Masahiro, & Noda, Tetsuji. (2007). Formation of silicon nanowires by CVD using gold catalysts at low temperatures. *Materials transactions*, 48(8), 2202-2206.
- Tabata, Akimori, & Komura, Yusuke. (2007). Preparation of nanocrystalline cubic silicon carbide thin films by hot-wire CVD at various filament-to-substrate distances. *Surface and Coatings Technology*, 201(22), 8986-8990.
- Tange, Shinya, Inoue, Keisuke, Tonokura, Kenichi, & Koshi, Mitsuo. (2001). Catalytic decomposition of SiH<sub>4</sub> on a hot filament. *Thin Solid Films*, 395(1), 42-46.
- Trwoga, PF, Kenyon, AJ, & Pitt, CW. (1998). Modeling the contribution of quantum confinement to luminescence from silicon nanoclusters. *Journal of applied physics*, 83(7), 3789-3794.
- Wagner, RS, & Ellis, WC. (1964). Vapor-liquid-solid mechanism of single crystal growth. *Applied Physics Letters*, 89-90.
- Wan, Y, Sha, J, Chen, B, Fang, Y, Wang, Z, & Wang, Y. (2009). Recent Pat: Nanotechnol.
- Wang, Bing, Wang, Yingde, Lei, Yongpeng, Wu, Nan, Gou, Yanzi, Han, Cheng, & Fang, Dong. (2014). Hierarchically porous SiC ultrathin fibers mat with enhanced mass transport, amphipathic property and high-temperature erosion resistance. *Journal of Materials Chemistry A*, 2(48), 20873-20881.

- Wang, Dong-Hua, Xu, Di, Wang, Qing, Hao, Ya-Juan, Jin, Guo-Qiang, Guo, Xiang-Yun, & Tu, KN. (2008). Periodically twinned SiC nanowires. *Nanotechnology*, 19(21), 215602.
- Wang, N, Tang, YH, Zhang, YF, Lee, CS, Bello, I, & Lee, ST. (1999). Si nanowires grown from silicon oxide. *Chemical physics letters*, 299(2), 237-242.
- Westwater, John, Gosain, DP, Tomiya, S, Usui, S, & Ruda, H. (1997). Growth of silicon nanowires via gold/silane vapor–liquid–solid reaction. *Journal of Vacuum Science & Technology B*, 15(3), 554-557.
- Wiesmann, H, Ghosh, AK, McMahon, T, & Strongin, Myron. (1979). a-Si: H produced by high-temperature thermal decomposition of silane. *Journal of Applied Physics*, 50(5), 3752-3754.
- Willander, Magnus, Friesel, Milan, Wahab, Qamar-ul, & Straumal, Boris. (2006). Silicon carbide and diamond for high temperature device applications. *Journal of Materials Science: Materials in Electronics*, 17(1), 1-25.
- Wong, Eric W, Sheehan, Paul E, & Lieber, Charles M. (1997). Nanobeam mechanics: elasticity, strength, and toughness of nanorods and nanotubes. *Science*, 277(5334), 1971-1975.
- Wu, Yiying, & Yang, Peidong. (2001). Direct observation of vapor-liquid-solid nanowire growth. *Journal of the American Chemical Society*, 123(13), 3165-3166.
- Wu, Yue, Cui, Yi, Huynh, Lynn, Barrelet, Carl J, Bell, David C, & Lieber, Charles M. (2004). Controlled growth and structures of molecular-scale silicon nanowires. *Nano Letters*, 4(3), 433-436.
- Wu, Yue, Xiang, Jie, Yang, Chen, Lu, Wei, & Lieber, Charles M. (2004). Single-crystal metallic nanowires and metal/semiconductor nanowire heterostructures. *Nature*, 430(6995), 61-65.
- Xi, Guangcheng, Yu, Shijun, Zhang, Rui, Zhang, Meng, Ma, Dekun, & Qian, Yitai. (2005). Crystalline silicon carbide nanoparticles encapsulated in branched wavelike carbon nanotubes: synthesis and optical properties. *The Journal of Physical Chemistry B*, 109(27), 13200-13204.
- Xia, Younan, Yang, Peidong, Sun, Yugang, Wu, Yiying, Mayers, Brian, Gates, Byron, . . . Yan, Haoquan. (2003). One-dimensional nanostructures: synthesis, characterization, and applications. *Advanced materials*, 15(5), 353-389.

- Xiang, Jie, Lu, Wei, Hu, Yongjie, Wu, Yue, Yan, Hao, & Lieber, Charles M. (2006). Ge/Si nanowire heterostructures as high-performance field-effect transistors. *Nature*, 441(7092), 489-493.
- Yakimova, Rositsa, Petoral Jr, RM, Yazdi, GR, Vahlberg, Cecilia, Lloyd Spetz, Anita, & Uvdal, Kajsa. (2007). REVIEW ARTICLE: Surface functionalization and biomedical applications based on SiC. *Journal of Physics D Applied Physics*, 40, 6435-6442.
- Yan, HF, Xing, YJ, Hang, QL, Yu, DP, Wang, YP, Xu, J, . . . Feng, SQ. (2000). Growth of amorphous silicon nanowires via a solid-liquid-solid mechanism. *Chemical Physics Letters*, 323(3), 224-228.
- Yan, Ruoxue, Gargas, Daniel, & Yang, Peidong. (2009). Nanowire photonics. *Nature Photonics*, 3(10), 569-576.
- Yu, DP, Bai, ZG, Ding, Y, Hang, QL, Zhang, HZ, Wang, JJ, . . . Zhou, HT. (1998). Nanoscale silicon wires synthesized using simple physical evaporation. *Applied Physics Letters*, 72(26), 3458-3460.
- Yu, Linwei, O'Donnell, Benedict, Alet, Pierre-Jean, Conesa-Boj, S, Peiro, F, Arbiol, J, & i Cabarrocas, Pere Roca. (2009). Plasma-enhanced low temperature growth of silicon nanowires and hierarchical structures by using tin and indium catalysts. *Nanotechnology*, 20(22), 225604.
- Zeng, XB, Xu, YY, Zhang, SB, Hu, ZH, Diao, HW, Wang, YQ, . . . Liao, XB. (2003). Silicon nanowires grown on a pre-annealed Si substrate. *Journal of crystal growth*, 247(1), 13-16.
- Zhang, HZ, Yu, DP, Ding, Y, Bai, ZG, Hang, QL, & Feng, SQ. (1998). Dependence of the silicon nanowire diameter on ambient pressure. *Applied physics letters*, 73(23), 3396-3398.
- Zhang, Shu-Lin, Zhu, Bang-fen, Huang, Fuming, Yan, Yan, Shang, Er-yi, Fan, Shoushan, & Han, Weigiang. (1999). Effect of defects on optical phonon Raman spectra in SiC nanorods. *Solid state communications*, 111(11), 647-651.
- Zhou, XT, Wang, N, Lai, HL, Peng, HY, Bello, I, Wong, NB, . . . Lee, ST. (1999).  $\beta$ -SiC nanorods synthesized by hot filament chemical vapor deposition. *Applied physics letters*, 74(26), 3942-3944.
- Zou, Guifu, Dong, Chao, Xiong, Kan, Li, Hui, Jiang, Changlong, & Qian, Yitai. (2006). Low-temperature solvothermal route to 2H-SiC nanoflakes. *Applied physics letters*, 88(7), 1913.